Hedin, P., Almqvist, B., Berthet, T., Juhlin, C., Buske, S., Simon, H., Giese, R., Krauß, F., Rosberb, J.-E., Alm, P.-G. (2016): 3D reflection seismic imaging at the 2.5km deep COSC-1 scientific borehole, central Scandinavian Caledonides. - *Tectonophysics*, *689*, pp. 40—55.

DOI: http://doi.org/10.1016/j.tecto.2015.12.013

Tectonophysics 689 (2016) 40–55

Contents lists available at ScienceDirect

Tectonophysics

journal homepage: www.elsevier.com/locate/tecto

3D reflection seismic imaging at the 2.5 km deep COSC-1 scientific borehole, central Scandinavian Caledonides

Peter Hedin [a,*], Bjarne Almqvist [a], Théo Berthet [a], Christopher Juhlin [a], Stefan Buske [b], Helge Simon [b], Rüdiger Giese [c], Felix Krauß [c], Jan-Erik Rosberg [d], Per-Gunnar Alm [d]

[a] Department of Earth Sciences, Uppsala University, Uppsala, Sweden
[b] Institute of Geophysics and Geoinformatics, TU Bergakademie Freiberg, Freiberg, Germany
[c] Scientific Drilling, Helmholtz Centre Potsdam GFZ German Research Centre for Geosciences, Potsdam, Germany
[d] Engineering Geology, Lund University, Lund, Sweden

ARTICLE INFO

Article history:
Received 16 July 2015
Received in revised form 4 December 2015
Accepted 16 December 2015
Available online 30 December 2015

Keywords:
3D reflection seismic
Continental scientific deep drilling
Borehole geophysics
Collisional orogeny in the Scandinavian Caledonides
Seve Nappe Complex
Shear zones

ABSTRACT

The 2.5 km deep scientific COSC-1 borehole (ICDP 5054-1-A) was successfully drilled with nearly complete core recovery during spring and summer of 2014. Downhole and on-core measurements through the targeted Lower Seve Nappe provide a comprehensive data set. An observed gradual increase in strain below 1700 m, with mica schists and intermittent mylonites increasing in frequency and thickness, is here interpreted as the basal thrust zone of the Lower Seve Nappe. This high strain zone was not fully penetrated at the total drilled depth and is thus greater than 800 m in thickness.

To allow extrapolation of the results from downhole logging, core analysis and other experiments into the surrounding rock and to link these with the regional tectonic setting and evolution, three post-drilling high-resolution seismic experiments were conducted in and around the borehole. One of these, the first 3D seismic reflection land survey to target the nappe structures of the Scandinavian Caledonides, is presented here. It provides new information on the 3D geometry of structures both within the drilled Lower Seve Nappe and underlying rocks down to at least 9 km.

The observed reflectivity correlates well with results from the core analysis and downhole logging, despite challenges in processing. Reflections from the uppermost part of the Lower Seve Nappe have limited lateral extent and varying dips, possibly related to mafic lenses or boudins of variable character within felsic rock. Reflections occurring within the high strain zone, however, are laterally continuous over distances of a kilometer or more and dip 10–15° towards the southeast. Reflections from structures beneath the high strain unit and the COSC-1 borehole can be followed through most of the seismic volume down to at least 9 km and have dips of varying degree, mainly in the east–west thrust direction of the orogen.

1. Introduction

The Scandinavian Caledonides represent one of the best preserved inactive orogens in the world in which to study thrust tectonics (Asklund, 1960; Gee, 1978; Hossack and Cooper, 1986; Törnebohm, 1888) and extensional tectonics (Andersen, 1998; Fossen, 2000). The orogen initiated in the late Ordovician by closure of the Iapetus Ocean and subsequent continental collision between Laurentia and Baltica in Silurian times (Gee et al., 2008). By the end of its formation, in early to middle Devonian (Gee et al., 2008; Rey et al., 1997), the mountain range was comparable in several aspects to the present day Himalayan-Alpine orogen (e.g. Andersen, 1998; Gee et al., 2010; Labrousse et al., 2010). Today's surface corresponds to mid crustal levels of the paleo-orogen, exposed through erosion, uplift and extension. Thus, we can study well preserved remnants of key orogenic features and their associated processes from the core of the mountain belt at the surface or just below it.

Remnants of the Caledonides in the present Scandinavian mountain belt, the Scandes, have been the subject of intense geological and geophysical investigations over the past 40 years (e.g. Corfu et al., 2014; Gee and Sturt, 1985; Gee, 1975; Gee et al., 2008; Roberts, 2003; Stephens and Gee, 1989). Much focus has been along a profile through

Abbreviations: BL, Byxtjärn-Liten 2D reflection seismic profile (Hedin et al., 2012); CCT, Central Caledonian Transect; COSC, Collisional Orogeny in the Scandinavian Caledonides; ICDP, International Continental Scientific Drilling Program; KF, Kallsjön-Fröå 2D reflection seismic profile (Hedin et al., 2012); SNC, Seve Nappe Complex; SSDP, Swedish Scientific Drilling Program.

* Corresponding author at: Department of Earth Sciences, Applied Geophysics, Villavägen 16, 75236 Uppsala, Sweden.
E-mail addresses: peter.hedin@geo.uu.se (P. Hedin), bjarne.almqvist@geo.uu.se (B. Almqvist), theo.berthet@geo.uu.se (T. Berthet), christopher.juhlin@geo.uu.se (C. Juhlin), buske@geophysik.tu-freiberg.de (S. Buske), helge.simon@geophysik.tu-freiberg.de (H. Simon), rudi@gfz-potsdam.de (R. Giese), felix.krauss@gfz-potsdam.de (F. Krauß), jan-erik.rosberg@tg.lth.se (J.-E. Rosberg), per-gunnar.alm@tg.lth.se (P.-G. Alm).

http://dx.doi.org/10.1016/j.tecto.2015.12.013

the central Scandes, crossing the mountain belt from east of the Caledonian thrust front in the province of Jämtland, Sweden, to the coast of the Norwegian province of Tröndelag (Fig. 1, Dyrelius et al., 1980). A major reflection seismic survey along the so called Central Caledonian Transect (CCT) revealed a very reflective upper crust (Hurich, 1996; Hurich et al., 1989; Juhojuntti et al., 2001; Palm et al., 1991). Additional seismic

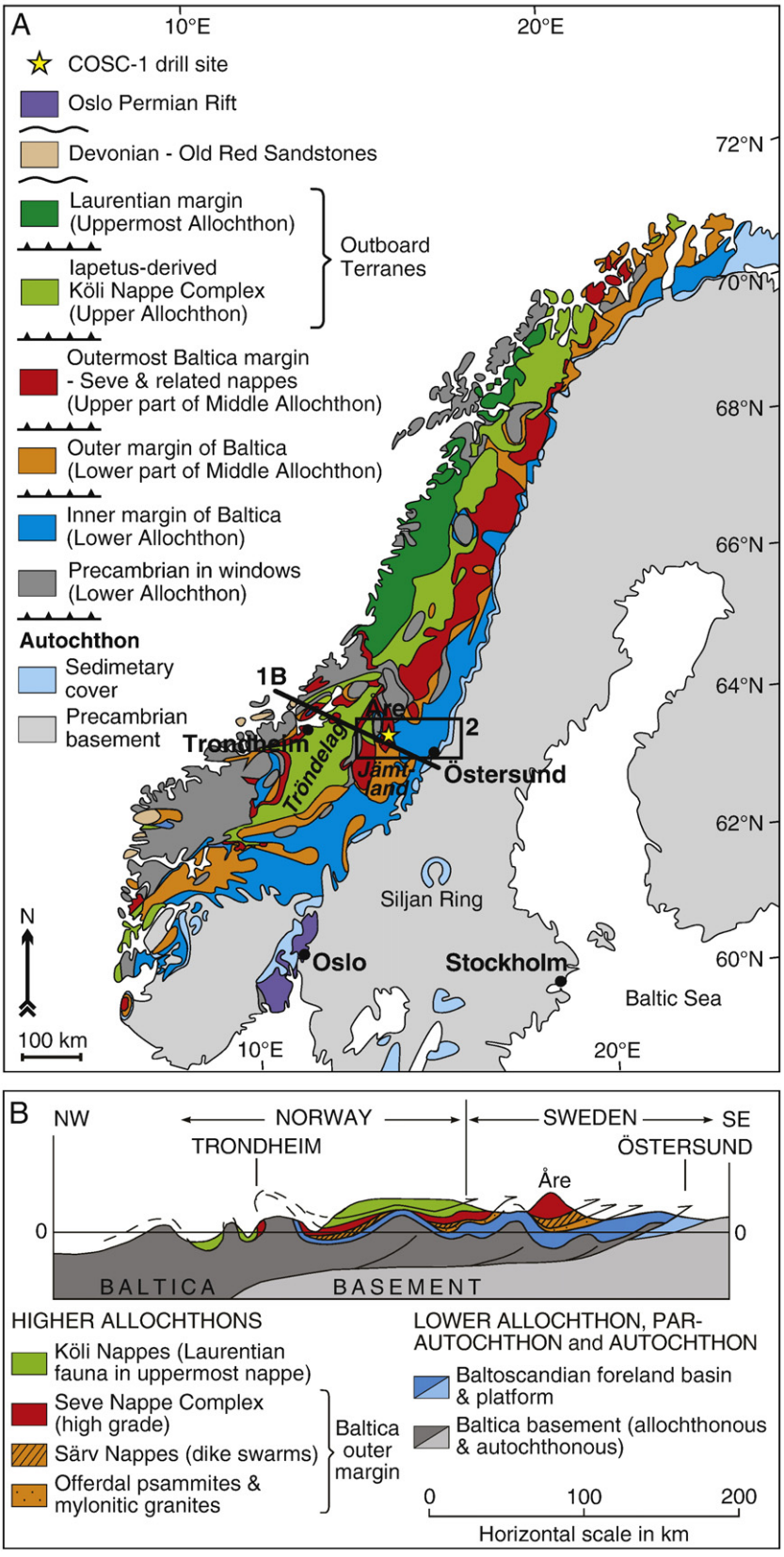

Fig. 1. A) Tectonostratigraphic map of the Scandinavian Caledonides (modified from Gee et al., 1985). The black rectangle shows the location of the map in Fig. 2. B) Schematic cross section along the black line in (A), showing the configuration of thrust emplaced nappes.

(e.g. England and Ebbing, 2012; Hedin et al., 2012; Palm, 1984; Schmidt, 2000), potential field (Dyrelius, 1986; Dyrelius, 1980; Ebbing et al., 2012; Elming, 1988; Hedin et al., 2014; Pascal et al., 2007) and magnetotelluric (Korja et al., 2008) investigations in the same area have helped to improve the large scale interpretation of the crust beneath the Caledonides of central Scandinavia.

In recent years, more focus has been placed on key questions concerning the conditions and processes during the active formation of the mountain belt, such as the emplacement of hot allochthons (Grimmer et al., 2015; Ladenberger et al., 2014) and generation and exhumation of ultra high pressure (UHP) rocks (Majka et al., 2014). Due to the inaccessibility of exposed outcrop, these questions are suitably answered through drilling and direct sampling of the subsurface. The Collisional Orogeny in the Scandinavian Caledonides (COSC) project (Gee et al., 2010; Lorenz et al., 2011) is led by the Swedish Scientific Drilling Program (SSDP) with support from the International Continental Scientific Drilling Program (ICDP). The project aims to improve our understanding of orogenic processes and investigate the current state of the Scandinavian Caledonides through scientific deep drilling. The lower units of the high-grade metamorphic Seve Nappe Complex (SNC), with evidence of deep subduction and ductile deformation and transportation (Klonowska et al., 2014; Ladenberger et al., 2014), was selected as the first target (COSC-1; Gee et al., 2010).

The COSC-1 borehole was drilled on the eastern flank of the Åreskutan synform close to the town of Åre in western Jämtland (ICDP drill site 5054–1-A, Figs. 1A and 2) between May and August 2014. Except for the uppermost 103 m, where conductor casing was installed prior to drilling, the hole was fully cored with >99% core recovery down to a final driller's depth of 2496 m (Lorenz et al., 2015b). A continuous geological section through the Lower Seve Nappe and into underlying mylonites was thus obtained, complemented by a comprehensive suite of geophysical and geochemical data from logging of the core and borehole (Lorenz et al., 2015b).

Imaging the structures away from the borehole in high resolution is of great importance to allow extrapolation of downhole logging results, core analysis and other geological and geophysical experiments into the formation surrounding the borehole. High resolution 2D seismic reflection profiles, acquired in 2010, were used to locate the most suitable place for drilling (Hedin et al., 2012). These profiles provided detailed images of the subsurface and, together with the previously acquired CCT profile and potential field data, allowed for a first 3D interpretation of the major tectonic units in the area (Hedin et al., 2012, 2014). The structures within the lower SNC were, however, not clearly imaged in the 2D sections. One likely possibility for this is the complex 3D geometry of the structures within this unit, which is not handled properly in 2D processing and also causes significant scattering of seismic energy. This is supported by crossdip analysis and swath 3D processing by Hedin (2015). Furthermore, the COSC-1 drill site was located near the very edge of available seismic data, far from the 2D binning geometry, introducing further uncertainties for interpretation of the complex geometry of structures (Hedin, 2015).

Following the completed drilling, a major seismic survey with multiple experiments was carried out in the COSC-1 borehole and surrounding area (Lorenz et al., 2015b). One component of the survey was the first ever, albeit limited, 3D reflection seismic acquisition on land in Scandinavia to target the Caledonian Nappe structures. Limited, in this case, refers to an incomplete coverage of source locations (which followed available roads in the area) and the resulting imperfect distribution of common midpoints (CMP). In this paper we present results from the high resolution seismic imaging of the SNC and deeper structures in the vicinity of the COSC-1 borehole. Delineation of major reflectivity and a first correlation with preliminary data from downhole

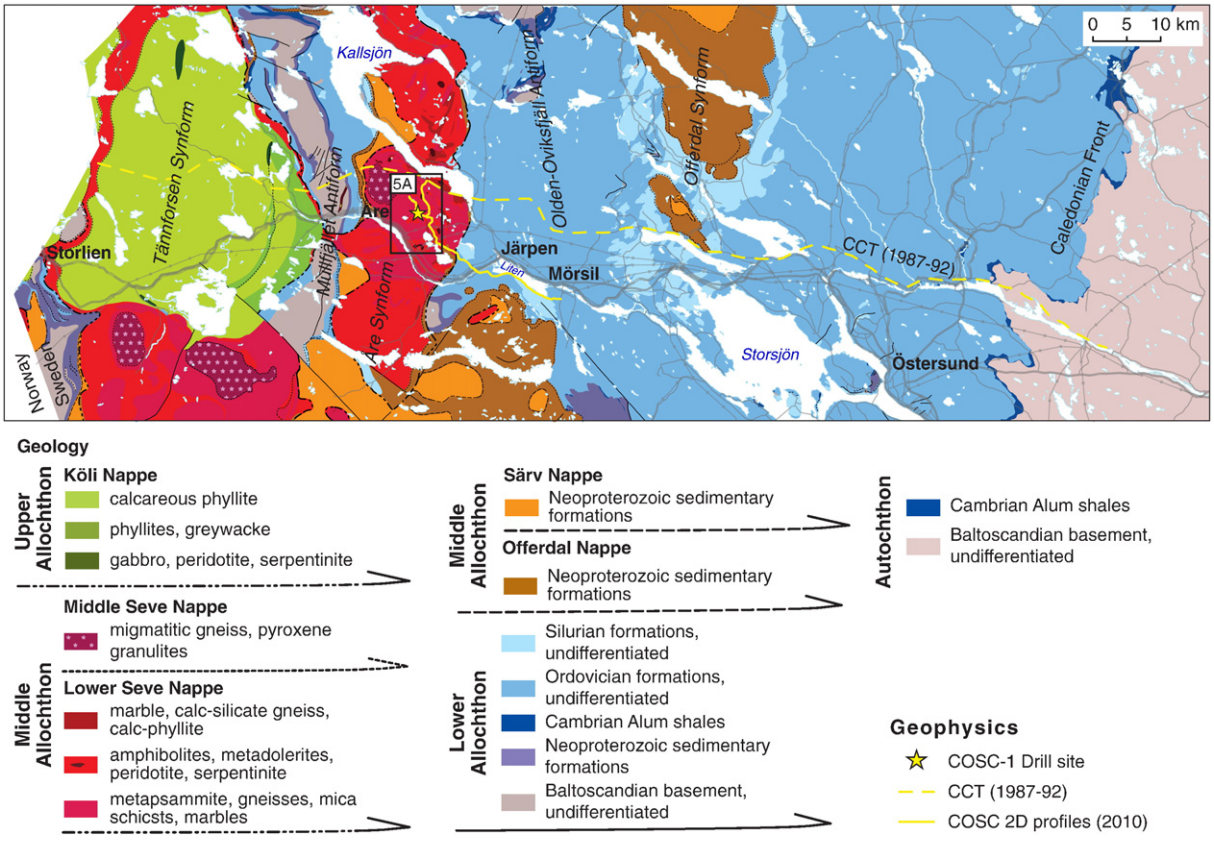

Fig. 2. Regional bedrock geological map along the Swedish part of the Central Caledonian Transect (based on the bedrock geological map of Sweden, © Geological Survey of Sweden [I2014/00601] and Strömberg et al., 1984) showing the tectonostratigraphic relationship between the thrust nappes and the NS trending folds that characterize the area. The black rectangle shows the location of the map in Fig. 5A.

logging and core analysis provide new insight on the history and nature of the Seve Nappe Complex.

2. Geological setting

2.1. Geology of the Seve Nappe Complex (SNC)

The Middle Allochthon of the Scandinavian Caledonides, comprising units originating from the outer margin of the Baltica plate (Fig. 1; Gee, 2015), hosts the Seve Nappe Complex, which consists in general of granulite and amphibolite facies metamorphosed rocks derived from the continent-ocean transition zone (Gee et al., 2013). The SNC has been further divided into upper, middle and lower subunits (Fig. 2). The Upper Seve Nappe (not present in the study area) consists of amphibolite grade metasediments, and is tectonostratigraphically bounded by the overlying Köli Nappe Complex, which is part of the Upper Allochthon with rocks derived from the former Iapetus Ocean (Fig. 2). Representative lithologies of the Upper Seve Nappe are amphibolites and mica-schists, occurring as imbricate slices emplaced at amphibolite grade conditions (Bergman and Sjöström, 1997). The transition from Upper to Middle Seve is marked mainly by the increasing grade of metamorphism shown by the latter subunit.

The middle subunit is considered to have reached highest metamorphic grade during the subduction phase of the Scandian orogeny, and consists mainly of granulite and eclogite facies metasediments and a lesser proportion of meta-igneous rocks, such as amphibolites and metagabbro (Fig. 2). During exhumation of this subunit it underwent extensive decompressional melting, which is evident from the near ubiquitous migmatization in the Middle Seve Nappe (Arnbom, 1980; Klonowska et al., 2014). Recent discoveries of micro-diamond inclusions in garnets in the Middle Seve Nappe, combined with geothermobarometry and thermodynamic equilibrium assemblage modeling, indicate that this subunit underwent ultrahigh pressure metamorphism (Majka et al., 2014; Klonowska et al., 2015). Several absolute ages have been reported from the Åreskutan mountain (located nearly 6 km to the west of the COSC-1 drill site) on migmatite and associated rocks, ranging from 423 ± 13 Ma to 455 ± 11 Ma (Gromet et al., 1996; Klonowska et al., 2014; Ladenberger et al., 2014; Majka et al., 2012; Williams and Claesson, 1987). The large spread in ages indicates that minerals developed at different stages in the history of the Seve Nappe Complex with the older ages being related to monazite growth during the subduction of the SNC, prior to exhumation, and the younger ages being related to monazite growth at the base of the Middle Seve Nappe during the final stages of emplacement at mid-crustal levels within the orogen.

The transition from the Middle to the Lower Seve Nappe is marked by a basal ductile shear zone. On Åreskutan mountain the thickness of the transitional shear zone has been mapped to be about 50 m (Arnbom, 1980; Majka et al., 2012). Here, the Lower Seve Nappe is composed of upper greenschist facies and amphibolite grade metasediments and meta-igneous rocks. The major lithologies consist of felsic gneisses and calc-silicates, amphibolites, and mica-schists (sometimes garnet-bearing), as well as occasional meta-gabbro and marble. All lithologies encountered in the Lower Seve Nappe are clearly deformed and subhorizontally layered with local tight folding. The layered and stretched gneisses and boudinaged amphibolites can be observed in outcrop localities in close vicinity to the COSC-1 borehole (Fig. 3A). There is clear evidence for melt-migration having occurred in the Lower Seve, as evidenced by felsic leucosome cross-cutting both the layered gneisses and amphibolites. Few absolute ages have been reported from the Lower Seve Nappe, but Gromet et al. (1996) used the U-Pb method to date titanite in calc-silicate and amphibolite, yielding ages that range from 437 to 427 Ma. The base of the Lower Seve Nappe is marked by a transition to the Särv and Offerdal Nappes, which comprise the lower units of the Middle Allochthon (Figs. 1 and 2). The Särv Nappe consists mainly of greenschist facies metasandstone that is cross-cut by 600 Ma rift-related dolerite dikes. The bottom of Särv is marked by a basal thrust zone with rotation and straining of the dolerite dykes in concordance with the foliation (Gilotti and Kumpulainen, 1986). The Offerdal nappe consists of highly deformed, finely banded and sometimes isoclinally folded sandstones and conglomerates, which are inferred to be of Neoproterozoic age (Gee et al., 2014).

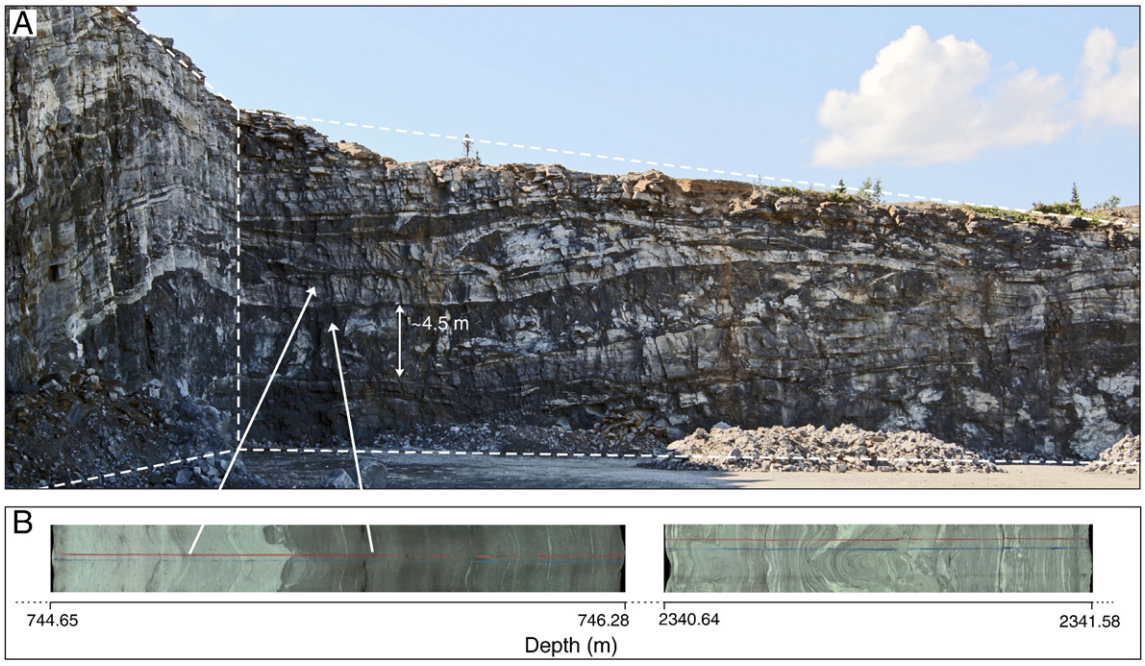

Fig. 3. A) Amphibolite boudins (dark) surrounded by felsic gneisses (light) in a quarry located about 4 km SE of the COSC-1 drill site. B) Two unrolled core-scans (360° imaging) showing a typical transition from gneiss to amphibolite in the upper part of the borehole (ICDP sections 5054–1-A-228Z-1WR (IGSN: 10273/ICDP5054ESVT001) and 5054–1-A-228Z-2WR (IGSN: 10273/ICDP5054ESWT001)) and a section of mylonite near the base of the borehole (ICDP section 5054–1-A-671Z-4WR (IGSN: 10273/ICDP5054ESSL201)).

2.2. The COSC-1 core and borehole

Based on the lithological description, the drill core can be divided into two parts (Fig. 4A; Lorenz et al., 2015b). The uppermost part, from 102.4 m to 1710 m depth, consists of alternating layers of felsic calc-silicates/gneisses and amphibolites. Fig. 3B shows, on the left, an unrolled core-scan of a core section from a depth of around 745 m with a sharp transition between typical gneiss and amphibolite. Occasional layers of metagabbro (10 to 30 m thick) occur between c. 500 to 1000 m.

In the lowermost part, at depths greater than 1710 m, the lithologies become increasingly mylonite-dominated. This indicates strong deformation, although the localization of strain seems to be broadly distributed because the thickness of the zone is at least 800 m. However, the intermittent occurrence of the mylonites surrounding zones of less deformed rock (mainly gneisses and amphibolites) suggest that they may have developed as anastomosing shear zones (e.g., Arbaret et al., 2000), or deformation lenses. In this case the deformation has been localized into narrow bands, rather than having developed as a single thick shear zone. Typical mylonite from a depth of about 2340 m is shown in Fig. 3B (right). The deepest mafic rock is encountered at 2314 m depth and metasandstones are present below depths of c. 2350 (Lorenz et al., 2015b). Although the affinity of the latter is yet to be determined, they suggest a transition from the Lower Seve Nappe into lithologies of the underlying units (though still strongly mylonitized) occurs at this depth.

Felsic veins (pegmatite), composed mainly of quartz and feldspar, occur throughout the drill core and are generally on the order of a few cm to 10s of cm thick, rarely exceeding one meter thickness. The bedrock is generally intact, and few open (water-bearing) fractures are encountered in the borehole. Healed fractures do, however, occur frequently although their thicknesses are usually less than a cm.

In parallel with the drilling operations, the drill-core was logged on-site using a multi-sensor core-logger. This provided reliable measurements of density and magnetic susceptibility. However, on-core measurements of P-wave velocity (v_p) yielded inaccurate results and are therefore not considered for this study. Several borehole logging runs were conducted in the COSC-1 borehole during and after drilling operations, and included a range of different sondes (Lorenz et al., 2015b). Of particular interest to the current study are the measurements made with the sidewall density and compensated sonic sondes. Due to instrument limitations and logistics, these density and velocity data from downhole measurements are limited to depths ranging from about 105 m to 1605 m.

The downhole logs were depth matched using as a continuous reference the total natural gamma log (Lorenz et al., 2015a). Depth matching of the on-core with the downhole logs was done using the continuous measurements of magnetic susceptibility. The on-core and in-situ density logs show a very good correlation (Fig. 4A). A shift towards lower densities is observed in the on-core log as compared to the in-situ measurements (Fig. 4A) which is likely caused by three factors: 1) different instrumentation are used which gives a constant shift; 2) the on-core measurements are affected by edge effects that give a frequent occurrence of erroneously low density measurements which in turn affect the applied running average filter; and 3) removal of confining pressure after retrieval of core should give a shift towards lower densities that increases linearly with depth. The latter, if present, is too small to be observed in the data.

A large number of peaks are observed in the logs of density and v_p that can be correlated with thick units (several meters to tens of meters) with mafic lithologies surrounded by felsic rock. Two zones, between 175 to 180 m and 1200 to 1313 m, show secondary porosity and micro-carst development that correlate with negative spikes in the v_p log (Fig. 4A). The latter can also be linked to observed hydraulically conductive zones (Tsang et al., 2015).

Fig. 4B shows the P-wave velocity as a function of density, i.e. independent of depth and using unfiltered data from the downhole logging of the upper 1605 m. Two clear distributions in the data are

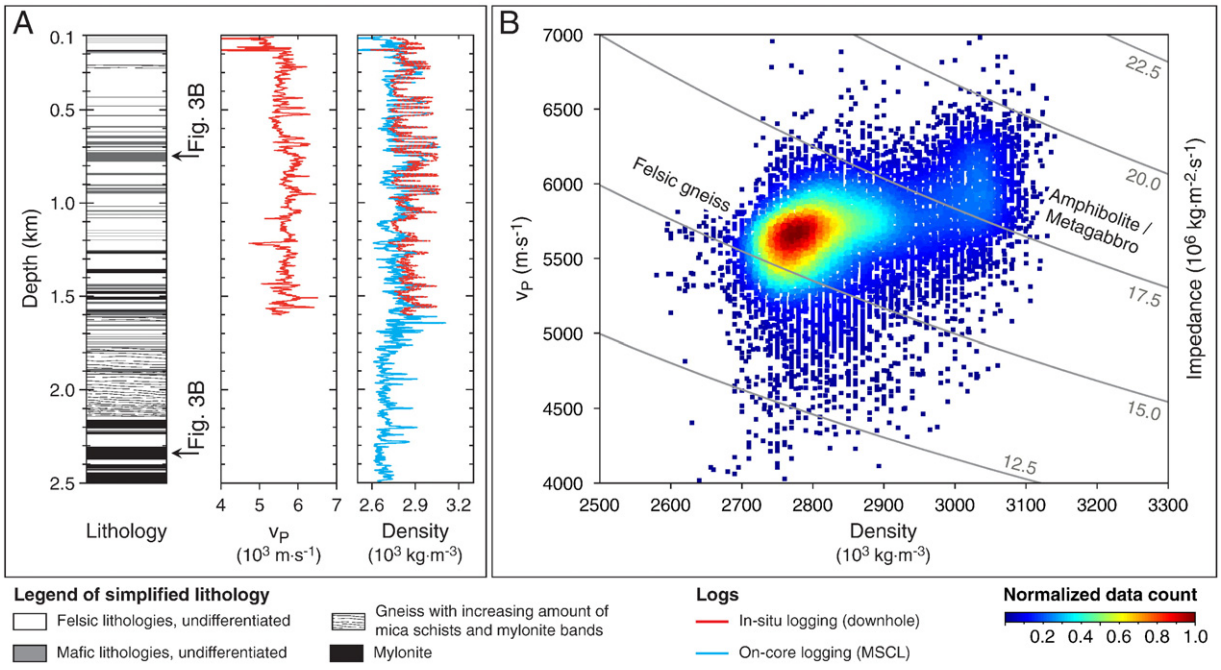

Fig. 4. A) On the left is a simplified lithological section based on initial on-site mapping of the retrieved core. For the purpose of visualization, lithologies have been roughly partitioned based on their dominant component as 1) felsic rocks (gneisses, calc-silicates, migmatites, marble and metasandstone), 2) mafic rocks (amphibolite and metagabbro), 3) gneisses with a large amount of mica schists and mylonite bands, and 4) mylonites. The depths of the two core sections in Fig. 3B are also marked. v_p and sidewall density are available from borehole logging between 105 and 1605 m depth while rock density from the core is available for the entire core (below 103 m). Peaks in density and v_p correlate well with the mafic lenses encountered in the core. The geophysical logs are shown after application of a 5 m running average. B) Crossplot of density vs. v_p shows a broad distribution around density and v_p of 2800 kg/m^3 and 5700 m/s, respectively, attributed to felsic rocks. A second distribution is observed around density and v_p of 3000 kg/m^3 and 6000 m/s, respectively, attributed to mafic rocks. Plotted in gray are the isolines of impedance showing that the impedance contrast between these two major lithological groups is about 2×10^6 kg/m^{2}s.

distinguished, a broad distribution around density and v_p of 2800 kg/m^3 and 5700 m/s, respectively, and a more concentrated distribution around density and velocity of 3000 kg/m^3 and 6000 m/s. This agrees well with a partitioning between felsic gneisses and calc-silicates, and the mafic rocks, primarily amphibolite and metagabbro.

3. The COSC-1 limited 3D seismic experiment

3.1. Acquisition

The seismic survey that was conducted in and around the COSC-1 borehole consisted of three separate experiments linked through recording the same source points. The first two components of this survey were a high resolution zero-offset Vertical Seismic Profile (VSP) (Krauß et al., 2015) and multi-azimuthal walkaway VSP with long offset surface recordings (Simon et al., 2015a). These used a combination of a receiver chain containing 15 three component 15 Hz geophones at 10 m separation and 180 three component 4.5 Hz geophones placed on the surface along three 2D profiles centered on the COSC-1 drill site. For the zero-offset VSP, the chain was moved at 2 m intervals, resulting in 1236 levels being recorded from 10 m to 2480 m (Krauß et al., 2015) and for the multi-azimuthal walkaway VSP it was moved between seven different levels in the borehole (Simon et al., 2015a). The third component of the survey was the limited 3D seismic dataset presented here. A stationary spread of 429 receivers (20 m separation along seven lines spaced 200 m apart), covering a surface area of about 1.5 km^2 around the COSC-1 drill site (Fig. 5A). This spread of receivers was kept active throughout the simultaneously running VSP experiments.

Rough terrain and infrastructure constrained the location of source points to roads in the area. Source points were therefore activated in a star pattern radiating outwards from the drill site to a maximum horizontal distance of about 5.2 km. A combination of a mechanical source (a rock breaking hydraulic hammer (VIBSIST, Cosma and Enescu, 2001), near offsets) and explosive charges (0.5 kg fired at 3.5–5 m depth, far offsets) were used. The nominal source point spacing was 20 m (VIBSIST) or 80 m (explosives) and the maximum horizontal source-receiver offset of the 3D experiment was about 5.75 km. An overview of the acquisition parameters is presented in Table 1. Note that about 57% of the explosive source shotholes were reused.

As the receiver chain of the multi-azimuthal walkaway VSP survey was moved between different levels, the VIBSIST source points were also activated up to five times with each repetition normally generating three sweeps. The shot holes for the explosive source points were filled with water for the first activation to minimize damage to the hole and to allow them to be reused. 73 out of 128 shot holes were reused for the second activation in which the holes were filled with gravel to increase the downgoing seismic energy.

Because each source point was repeatedly activated on different occasions, the total vertical stacking of the data is very high. Therefore, a harsh editing (>50%) of lower quality data (e.g. due to unfavorable weather conditions, environmental noise and breaks in the recording line, etc.) did not result in any significant loss of trace coverage in the final dataset. Seismic energy is strongly scattered within the targeted SNC and the signal strength decays rapidly with offset and penetrated depth. The S/N ratio of data generated with explosives is superior to VIBSIST generated data (even near offset), especially for imaging deeper structures (Fig. 6).

The rectangular binning geometry used for processing (Fig. 5B) covers an area of nearly 17 km^2 and encompasses all midpoints, but also contains large unsampled regions with about 57% of the CMP bins being empty. Fig. 5B shows the linear features of alternating high and low fold aligned with the receiver lines. As seen in the azimuth-offset distribution (Fig. 5C), the data also suffer from an irregular distribution

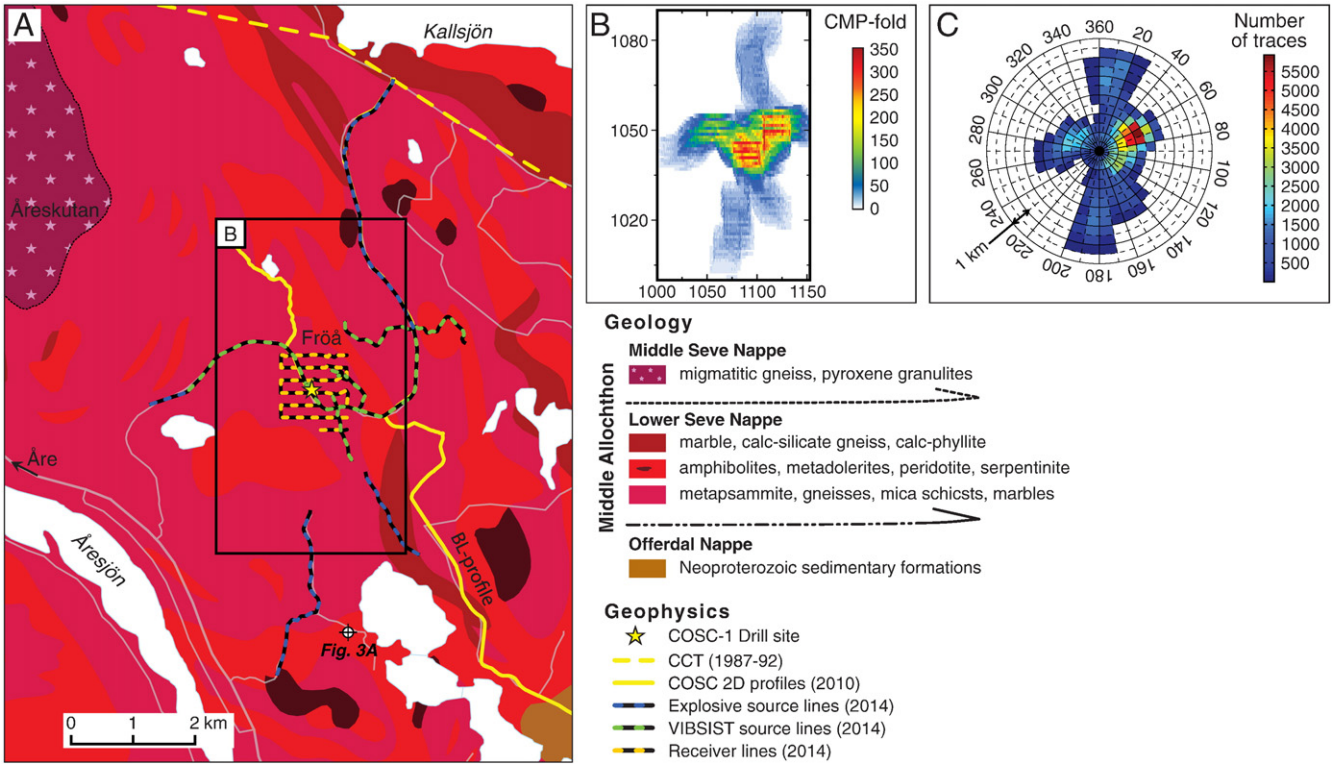

Fig. 5. A) Bedrock geology of the survey area (based on the bedrock geological map of Sweden, © Geological Survey of Sweden [I2014/00601] and Strömberg et al., 1984) with the limited 3D acquisition geometry. The black rectangle shows the lateral extent of the processing geometry further described in (B). The location of the quarry shown in Fig. 3A is also included. B) Processing geometry showing the extent of the seismic data volume and the fold distribution after rectangular binning of the midpoints into bins of 20 m (inline) by 60 m (crossline). The highest fold is in the central and eastern part of the volume and an acquisition footprint is observed with east–west directed linear features. C) Receiver-source offset-azimuth coverage of the 3D data showing that far offsets are limited primarily to the north–south direction.

Table 1
Acquisition parameters for the COSC-1 limited 3D survey.

Receiver spread type	Stationary spread
Number of channels	429
Receiver type	10 Hz, 1 Component
Receiver spacing	20 m
Receiver-line spacing	200 m
Source spread type	Star pattern
Source type	VIBSIST & Explosives
Source points	634
VIBSIST	
Source points	508
Excitations per source point	4–5
Sweeps per excitation	3
Hit interval for hammer	100–200 ms
Source spacing	20 m
Dynamite	
Source points	128
Excitations per source point	1–2
Explosive charge	0.5 kg
Source spacing	80 m
Near offset	0 m
Maximum offset	5748 m
Recording instrument	SERCEL 428 XL
Sample rate	1 ms
Record length	25 s
Field low cut	-
Field high cut	-
Data acquired	16/9–8/10, 2014

of azimuth and far offset. Far offset data are limited to narrow bands in mainly the N-S directions. Thus, the limited source point coverage in the acquisition geometry may cause a significant acquisition footprint which affects both lateral resolution and the capability to resolve dipping reflections (Cheraghi et al., 2012).

3.2. Processing

The data recorded using the VIBSIST source were decoded following the Swept Impact Seismic Technique (SIST) described by Park (1996) and Cosma and Enescu (2001). In some areas, the generation of strong surface waves in combination with rapid saturation of the source sweep to a constant hit frequency resulted in significant coherent noise in the data. Binning the hits according to hit interval during the decoding process slightly decreases this effect and the lower stacking power does not seem to decrease the signal strength in the decoded data. Data from source locations where more than one excitation was possible under favorable noise conditions were stacked to increase the signal to noise ratio.

Choice of Common Midpoint (CMP) binning geometry is important to limit the acquisition footprint from the non-standard 3D acquisition. After testing a few different binning strategies, the inline direction was chosen to be parallel with the receiver lines and a bin size of 20 by 60 m was used, with the longer side in the crossline direction. This resulted in smooth coverage and a high fold (Fig. 5B). A smaller bin size results in a lower and more variable fold with a lower S/N ratio and a stronger acquisition footprint. A larger bin size decreases the lateral resolution and limits the ability to correctly image dipping reflectors.

The processing of the data followed a standard processing sequence (as seen in Table 2) using a commercial seismic processing software package. Deconvolution, spectral equalization, spherical divergence compensation, automatic gain control (AGC) and different filters were applied to reveal reflections initially obscured by noise and unwanted signal, and enhance the signal from reflected arrivals before stacking. First arrivals produced considerable coherent noise at far offsets and were removed using a front mute. A typical common source gather from an explosive shot (source-receiver offsets ranging from 1.2 to 2.7 km) is shown in Fig 6 with refraction statics and trace balancing (Fig. 6A) compared to the full pre-stack processing except for the front mute (Fig. 6B). Fig. 6C and D show the same for one of the highest quality common source gathers for a VIBSIST excitation (source-receiver offsets ranging from 0.5 to 1.8 km). The superior S/N ratio of the explosive shots is apparent by comparing the two (Fig. 6). Stacking of data from only VIBSIST source points shows that they give little contribution to the image below about 5 km. Only the very strongest reflectors below 5 km are seen in the high fold areas and thus, the major contribution to the image below this depth comes from the explosive source points.

The biggest challenge during the processing stage was calculating accurate static corrections and several possibly contributing factors to this have been identified. These factors are: significant elevation differences for both receivers (<100 m) and source points (<250 m) due to the rugged topography, varying surface conditions and complex near surface structures, and limited acquisition over the structurally and lithologically complex unit. These elevation differences required shifting the data to a floating datum during processing, before using the final reference datum of 750 m above sea level.

Anisotropy has also been observed both in lab measurements (Wenning et al., 2015) and in the VSP experiments (Simon et al., 2015b). Residual static corrections had little effect on reflection coherency when applied to the entire dataset. Major improvement was, however, achieved through separating the data into ten subsets, based on source type and source-receiver azimuth, before calculating and applying the residual static corrections (Fig. 7). This was followed by a manual shift of the respective subsets (<10 ms) to match the major reflections, using the subset with explosive shots at shortest offset as a reference, before merging the subsets back into one dataset. However, the character of reflections at the edges of the subsets, especially where abrupt changes in fold are present due to the limited acquisition, differs slightly and is seen as vertical bands of reduced lateral continuity (Fig. 7). In the separate subsets, some of these bands are more pronounced after residual statics as the merging is not perfect, as seen in Fig. 7B. Thus, the processing is not surface consistent and uncertainties in depth have been introduced through the residual static calculations and subsequent manual shifts of separate data subsets.

Velocity analysis was done in several iterations to find the optimal root mean square (RMS) velocities for stacking. The initial focus was on the deeper continuous reflections so that accurate residual statics corrections could be calculated. Subsequent iterations focused on the SNC and underlying allochthons in the upper 1 s. 2D Coherency filtering (FX-Deconvolution) was applied after stacking, first in the inline direction and then in the crossline direction, to remove noise and artifacts introduced during the pre-stack filtering and stacking processes. This 2.5D filtering could potentially introduce artifacts, especially surrounding initially empty regions. To limit this, CMP bins that were initially empty were muted after each pass of the filtering.

Despite the problems with the static corrections, clear continuous lateral reflections are present in the stacked data (Fig. 8). These are particularly clear at depths coinciding with the high strain zone encountered in the COSC-1 borehole and below it. Fig. 8 also shows two time slices; one through a reflective region within the Lower Seve Nappe (Fig. 8C) and one through the deeper high strain zone (Fig. 8D). The acquisition footprint appears to be minimal in the time slices (Fig. 8C and D) as no linear features are present that are aligned with the east–west lines in the fold distribution (Fig. 5B). The higher fold in the central and eastern parts of the seismic volume allows slightly better imaging in these regions compared to the western part.

Migration is required since numerous dipping reflections are present within the SNC. Although pre-stack migration may have given a better result (assuming an accurate velocity model may be obtained), we settled for post-stack time migration using a finite difference algorithm because of its considerably lower computational requirements. Furthermore, only pseudo 3D migration was performed, essentially performing a 2D migration first in the inline direction and then in the crossline direction. This may also introduce artifacts from seismic energy migrated into initially empty regions. The stacked volume was padded with

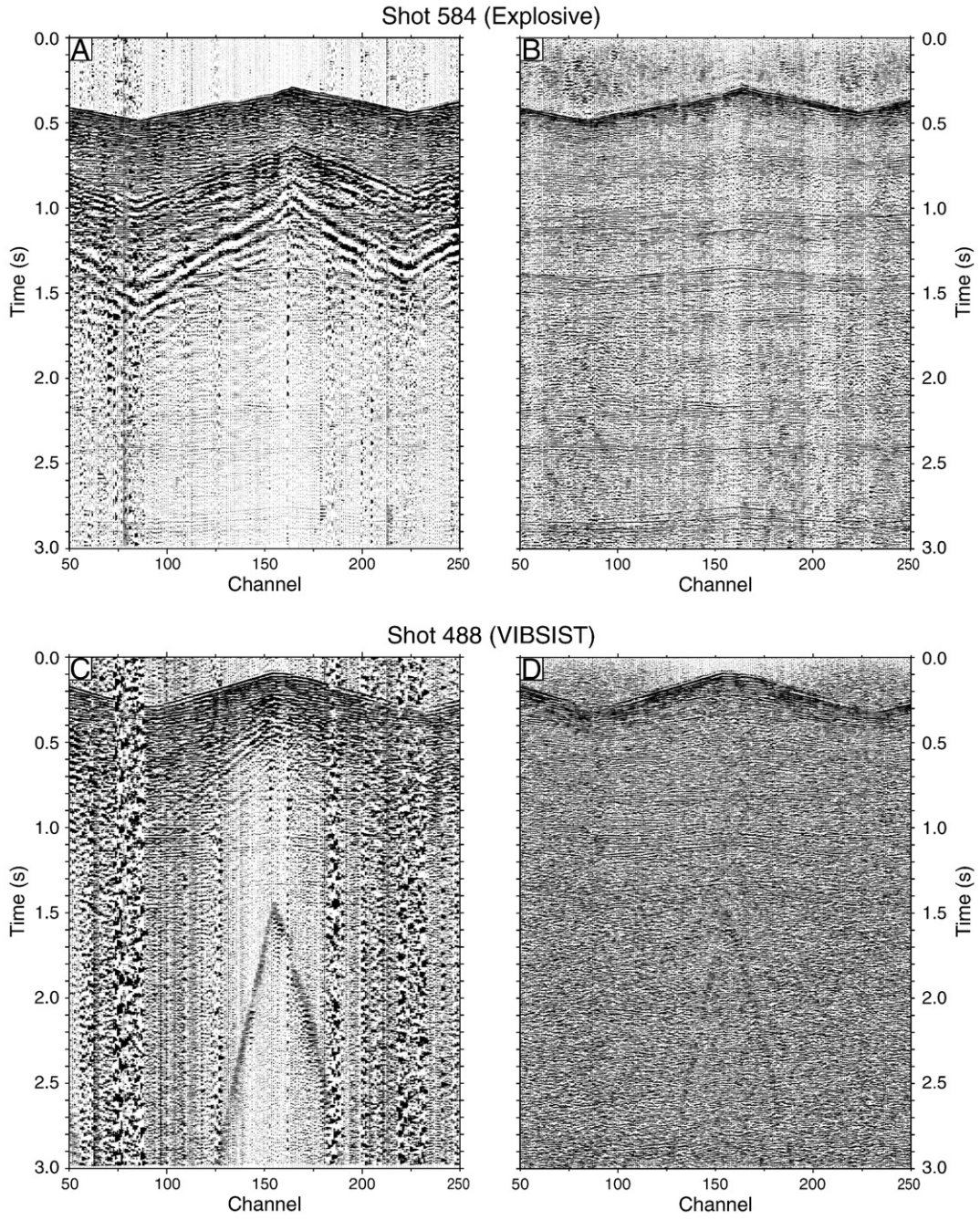

Fig. 6. A and B show an example of a common source gather (channels 50–250) from an explosive shot with 3 s of data. In A) refraction static corrections and trace balancing have been applied and B) shows the result after additional pre-stack processing steps except for front mute. Reflections are clearly visible throughout the entire gather. C and D show an example of a common source gather (channels 50–200) with the 3 s of decoded data from one of the highest quality VIBSIST excitations in terms of S/N ratio. C) has refraction statics and trace balancing applied, while D) has additional pre-stack processing steps with the exception of front mute. The VIBSIST data in C and D clearly have much weaker reflections than the explosive shot (A and B), and very little reflected energy below 1.5 s.

empty traces on all sides before migration to avoid wrap-around artifacts and initially empty traces were once more muted after migration. 3D Dip Moveout corrections (DMO) slightly improved the image in some areas, by correcting for conflicting dips and improving the continuity of some reflections. Other areas were degraded after DMO, possibly related to the vertical bands of reduced lateral continuity and imperfect merging of subsections after the initial residual static corrections. Migrating the stacked section without DMO corrections appears to give an overall clearer image with more coherent reflections both in the vertical and horizontal planes and this migrated volume has formed the basis for interpretation.

Finally, depth conversion was done on the seismic 3D volume to simplify the interpretation process and correlation with other geological and geophysical data. A velocity profile for depth conversion was based on averaging of interval velocities calculated directly from the zero-offset VSP data, assuming a vertical borehole and wave travel path (Krauß et al., 2015). Below 2.5 km depth this function is linearly increasing to 6100 m/s at 9 km depth. Inline 1045 is once more shown after migration and depth conversion in Fig. 9A. The 1D velocity function used for depth conversion is shown in Fig. 9B together with the simplified geological section and geophysical logs from the coring and logging of COSC-1.

Table 2
Processing steps and parameters.

Stacking of explosive data
Decoding and stacking of VIBSIST data
Manual trace editing
Refraction static corrections
Front mute
Airwave suppression filter
Spherical divergence compensation
Wiener deconvolution
filter length: 150 ms; gap length: 10–12 ms
Spectral equalization
15–30-120-180 Hz
Median velocity filter
1900, 2700, 3300 m/s
Band pass filter
0–700 ms 25–50-140-210 Hz
1000–1400 ms 20–40-120-180 Hz
1600–3000 ms 20–40-100-150 Hz
Trace balancing
AGC
Time window 200 ms
NMO correction
Residual static corrections
CMP stacking
Seismic reference datum: 750 m.a.s.l.
Coherency filtering (FX-Deconvolution)
Trace balancing
2.5D Finite difference time migration
θ_{max}: 53°
Time-to-depth conversion

4. Discussion

4.1. Reflection seismic data in relation to drilling results

As seen in Fig. 9A, the Lower Seve Nappe, including the high strain zone that was encountered in the COSC-1 borehole, as well as underlying rocks, are highly reflective. However, because of the complex geology of the SNC and the difficulty to properly correct for statics-related issues and conflicting dips, the reflection continuity is low, especially in the uppermost part. The minimum required separation of two reflectors to be distinguished is given by the vertical (parallel to normal incidence) and lateral (perpendicular to normal incidence) seismic resolution. These are normally defined by the one quarter of the dominant wavelength criteria and the width of the first Fresnel zone, respectively (Yilmaz, 2001). The Fresnel zone, which is related to the wavefront incident on a reflector, is in an anisotropic medium distorted into an elliptical shape that varies depending on the dip of the reflector giving a differential lateral resolution (Okoye and Uren, 1992). In reality, resolution is further degraded by low S/N ratios and the acquisition footprint as well as low reflection coefficients at the reflecting interface (Milkereit and Eaton, 1998; Salisbury et al., 2000). Resolving fine structure in crystalline rocks is therefore difficult because velocities are greater than 5000 m/s, reflection coefficients are generally low and targets often situated at significant depths (e.g. Adam et al., 2000). Taking the strong reflectivity in the lower part of the COSC-1 borehole, at a two-way-time of 0.8 s in Fig 9A, as an example and using an average vertical velocity of 6000 m/s and a dominant frequency of 50 Hz, the minimum vertical and lateral resolutions are 30 m and 380 m, respectively. Migration improves the lateral resolution, in t`heory to approximately the dominant wavelength (Yilmaz, 2001).

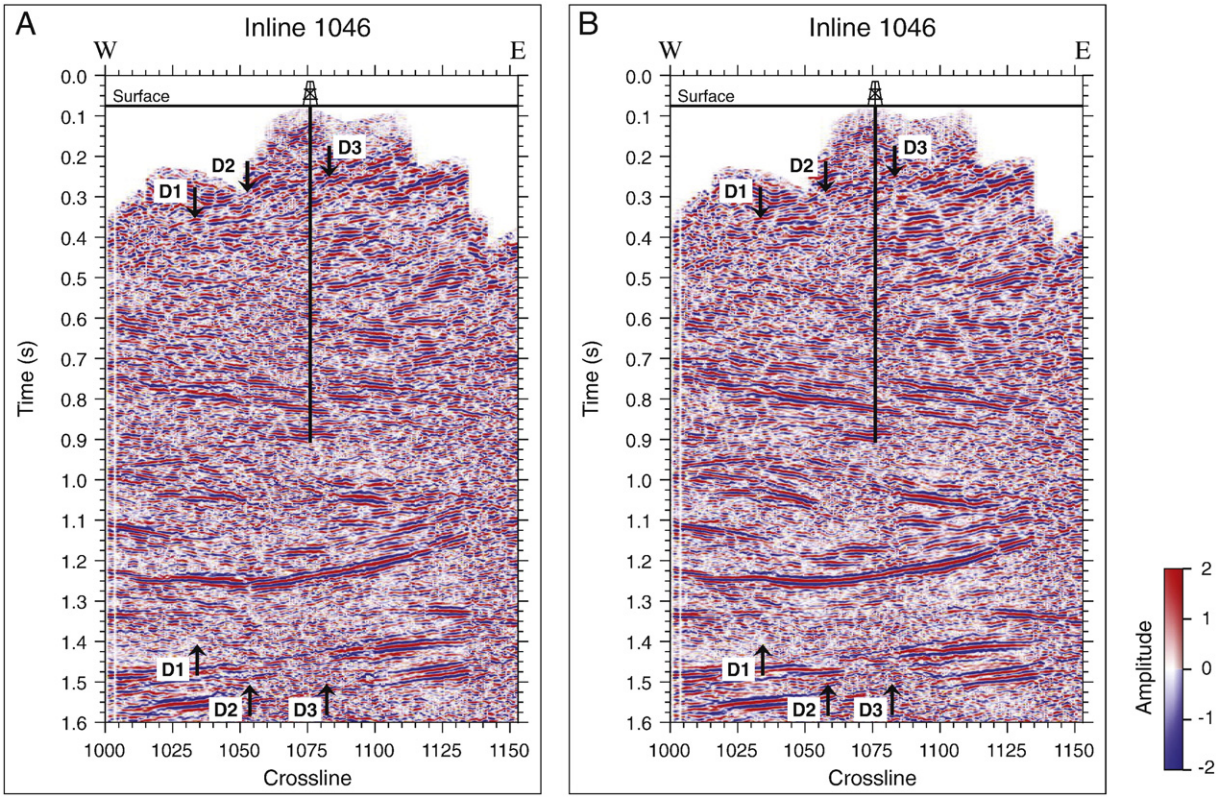

Fig. 7. Inline 1046 is shown for comparison of residual static corrections performed on (A) the full data set and (B) after splitting the data into subsets according to source type and source-receiver azimuth with subsequent remerging. Pre- and post-stack processing is the same. The overall improvement in reflection continuity seen in B is typical for the center of the seismic volume. Vertical bands of reduced reflection continuity, D1, D2 and D3, appear related to the limited acquisition and abrupt changes in fold and, in B, occur at the edges of the split subsets. Some of these vertical bands become more prominent in B due to inconsistent corrections between the subsets and imperfect merging in the overlapping regions.

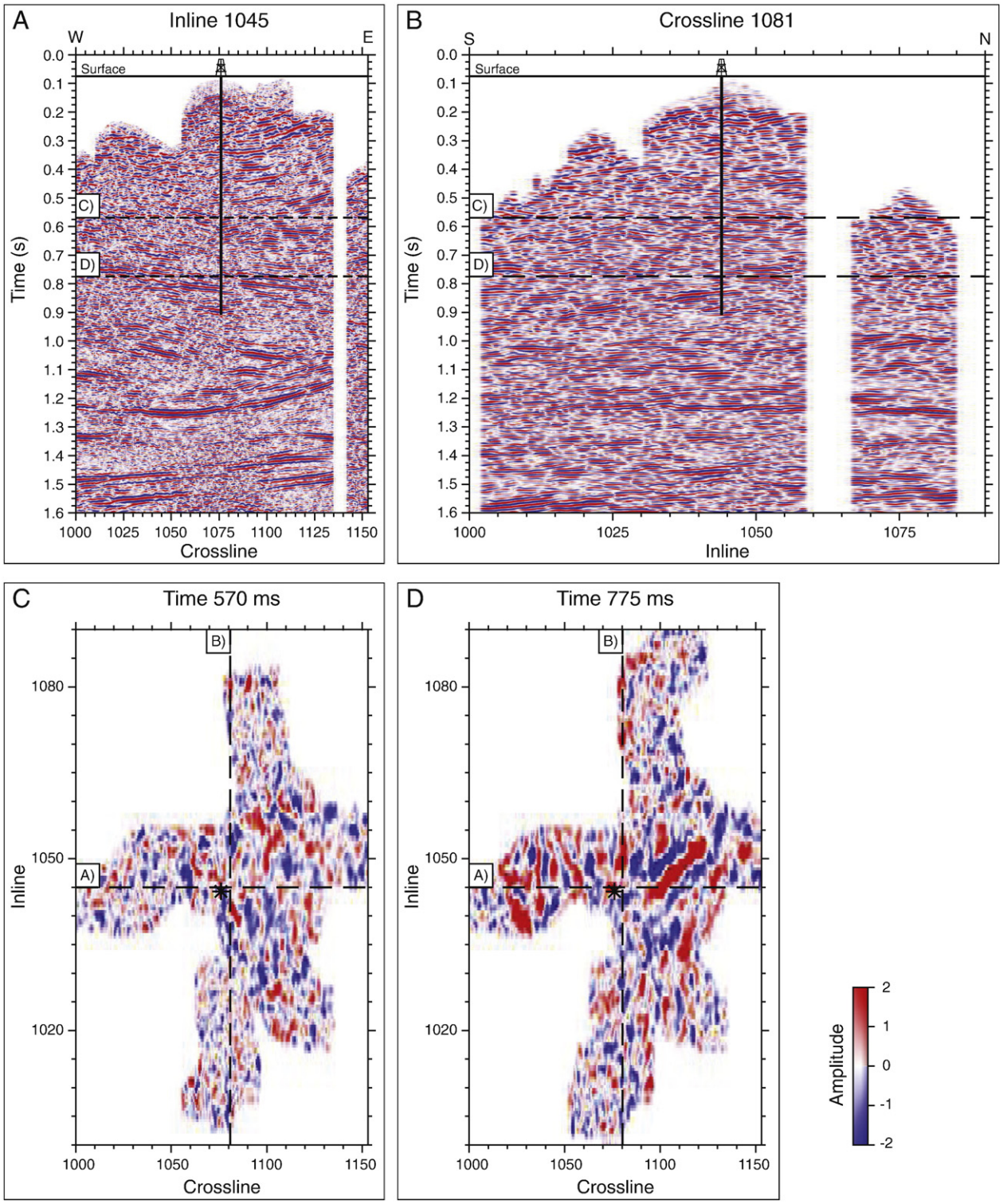

Fig. 8. Inline 1045 (A) and crossline 1081 (B) from the stacked cube intersect close to the COSC-1 drill site. The vertical line shows the approximate trajectory of the COSC-1 borehole and the two horizontal lines show the location of time-slices in (C) and (D). The two time-slices at 570 ms (C) and 775 ms (D) show a comparison of the limited lateral continuity of reflections within the SNC (C) with the longer continuity of reflections in the underlying mylonitic shear zone (D).

The on-core and in-situ logs were acquired with a 0.01 m sampling rate, in marked contrast to the seismic data. Therefore, a 5 m running average filter was applied to allow a more direct comparison with the seismic data and visualization as presented in Figs. 4A and 9B. An acoustic impedance log through the Lower Seve Nappe, between about 105 m and 1605 m depth, was calculated using the downhole measurements of density and v_p (Fig. 9B). The high variability in the log, even after filtering out the contribution from lithological variations less than 5 m thick, indicates numerous interfaces with significant impedance contrasts. In agreement with Fig. 4B, two main groups are observed that may be related to felsic (16×10^6 kg/m^{2}s) and mafic (18×10^6 kg/m^{2}s) lithologies (Fig. 9B). This contrast in acoustic impedance corresponds to a reflection coefficient of about 0.06. Under favorable noise conditions and with sufficient lateral continuity of

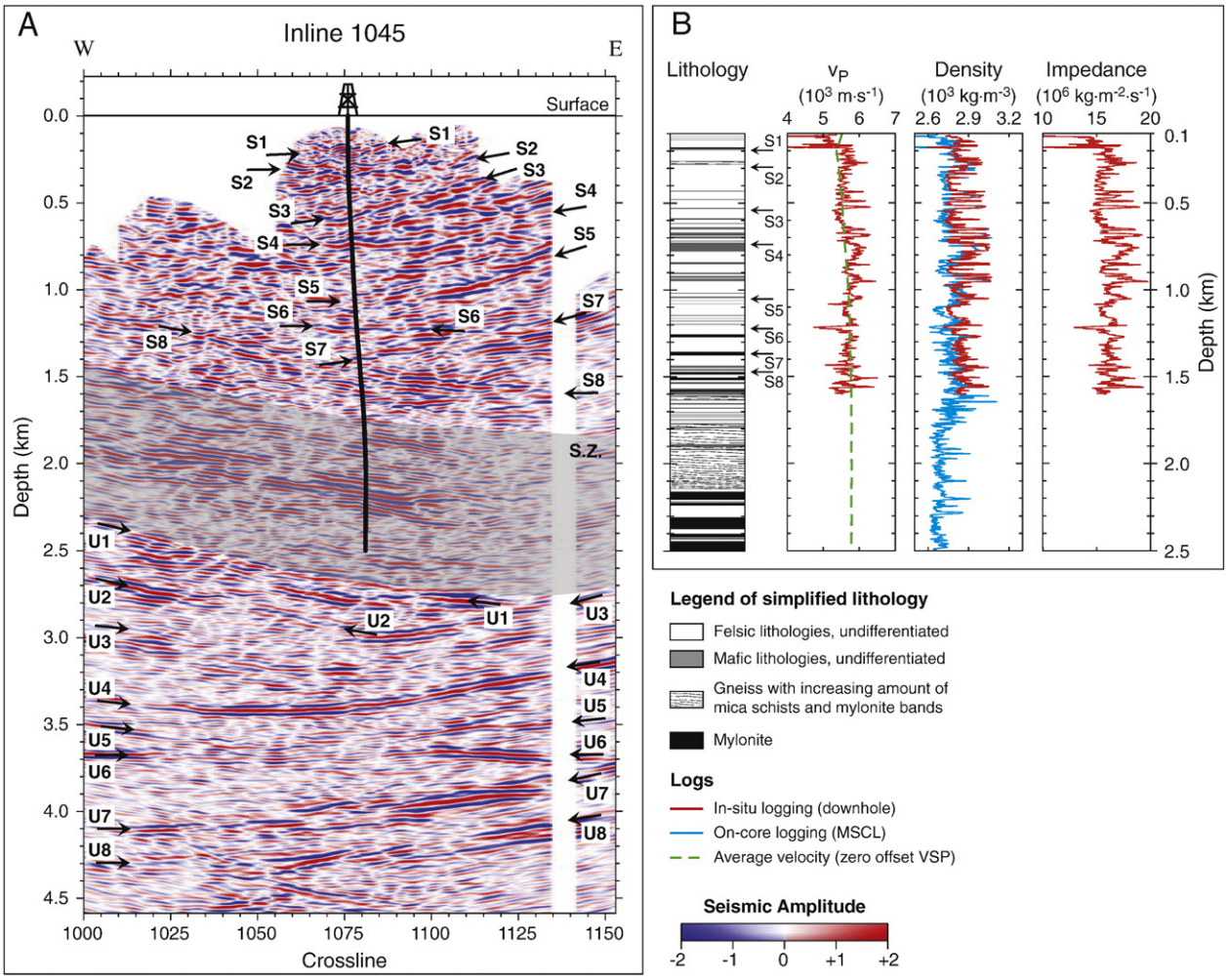

Fig. 9. A) Inline 1045 is shown after migration and depth conversion with the COSC-1 borehole trajectory deviating maximum 100 m eastwards. A distinct difference is observed in the reflectivity pattern above the shear zone (S.Z.), with limited lateral extent and conflicting dips, compared to within and below S.Z., with better defined geometry and lateral continuity. B) On the left, the upper 2.5 km of the 1D average velocity function used for time-to-depth conversion (based on velocities from the zero offset VSP) is shown together with the logged v_p. Below 2.5 km this function is a linear interpolation reaching 6100 m/s at 9 km depth. The acoustic impedance log shown on the right was calculated from the downhole logging of v_p and density. The impedance log shows an abundance of significant contrasts in the uppermost 1605 m and the density log from on-core measurements suggest that similar contrasts, but less frequent, occur in the deeper parts which agrees well with the observed reflectivity in (A). Depth is referenced to the surface elevation at COSC-1 (523 m above sea level). The geophysical logs are shown after application of a 5 m running average and are scaled vertically to match the true location along the borehole trajectory shown in (A).

interfaces, this would generate observable reflectivity (Salisbury et al., 2000). On the other hand the interfaces may be too frequent to be resolved in the reflection seismic data due to scattering and destructive interference.

Although no velocity data are provided by logging campaigns below 1.6 km, the zero-offset VSP experiment indicates several changes of velocity within the high strain zone, ranging from 6250 m/s to 5500 m/s. The density log from on-core measurements shows a general decrease in density below 1.7 km (Fig. 9B). Several sharp spikes related to mafic lenses within the mylonite dominated high strain zone, with density increases of up to 0.25 kg/m^3, are observed between 1.7 and 2.3 km depth. This suggests that equally strong but less frequent impedance contrasts also occur at these depths down to about 2.3 km depth. Density contrasts are less pronounced below 2.3 km (Fig. 9B), which could indicate that the interface between mylonite and meta-sandstone in the lowermost part of the high strain zone don't generate strong reflected energy, consistent with the weak reflectivity at corresponding depths (Fig. 9A).

The 1D velocity function used for depth conversion (Fig. 9B) is based on averaging the velocities from the zero-offset VSP experiment which gives a smooth conversion. It is, however, only representative in the vicinity of the COSC-1 borehole and involves some degree of uncertainty. Nevertheless, the reflectivity seen in Fig. 9A appears to correlate well with the geophysical logs and the geological section of Fig. 9B.

4.2. The COSC-1 limited 3D in relation to the 2D COSC seismic profile

Fig. 10 shows the intersection of inline 1052 with the 2D reflection seismic section from 2010. Reflections within the SNC high strain zone and in underlying rock match well even though the two data sets were acquired and processed independently. In the 2D data, reflectors below about 4.5 km beneath the SNC are not imaged due to lack of signal penetration, most probably due to scattering of seismic energy. These basement reflections are imaged in the new seismic 3D volume down to nearly 9 km, largely due to the contribution from the explosive source points. The strongest sub-horizontal reflection at about 6 km depth was, however, also clearly imaged in the shorter 2D profile of 2010 (KF in Hedin et al., 2012), and the reason why this reflection does not appear in the main 2D profile is unclear. Crossdip analysis and swath 3D processing of the 2D data gave only limited information on the 3D geometry of structures due to the narrow offset-azimuth coverage and low signal penetration through the SNC (Hedin, 2015). The new 3D data thus provides previously unavailable 3D information on

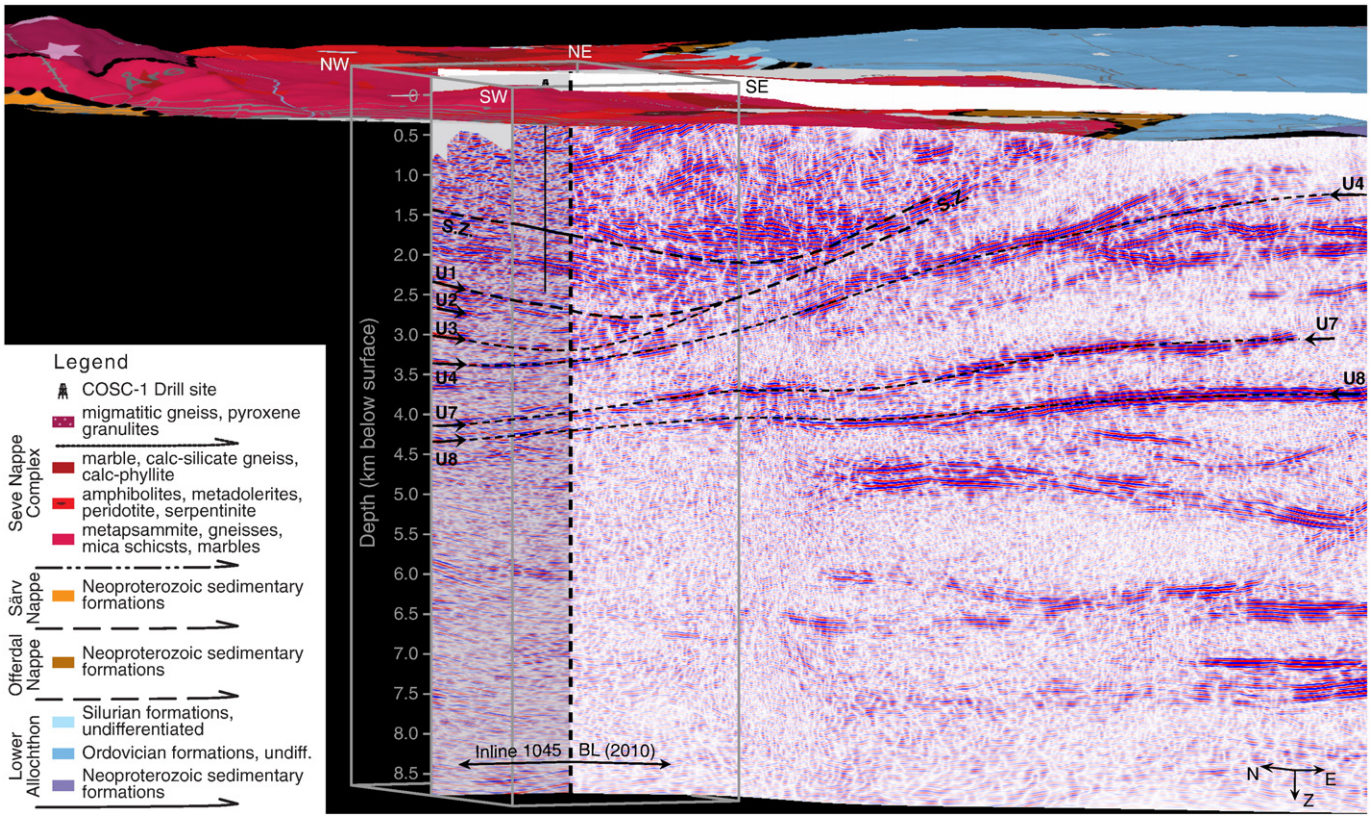

Fig. 10. A comparison of inline 1045 from the new 3D with the 2D seismic section BL (Hedin et al., 2012) where they intersect around crossline 1093 (vertical dashed line), viewed from SSW. Reflections within the SNC, although weaker and less continuous in the 3D seismic volume, show good correlation across the two datasets and the 3D seismic data allow constraining the geometry of reflectors in 3D. The good match between the datasets is clearly seen on the larger scale through the reflections at depths between 2.5 and 4.5 km depth. At greater depths, down to 9 km, reflections nearly indistinguishable in the 2D section can be traced laterally through most of the 3D seismic volume. Depth is referenced to the surface elevation at COSC-1 (523 m above sea level).

the structures both within the SNC as well as on deeper reflectors down to 9 km.

Reflections within the Lower Seve Nappe appear to be less continuous in the new 3D data as compared to the 2D section (Fig. 10). The limited stationary receiver spread constrains near offset traces to the center of the survey and also results in a lack of near surface information at some distance from the borehole. In comparison, the 2D data have a good distribution of near offsets along the acquisition line. Whereas the irregular fold of the 3D has a maximum of 318, but rarely exceeds 200, the fold distribution of the 2D profile is smooth with a maximum of 952 and rarely goes below 200, giving a much higher stacking power. With a narrower offset-azimuth distribution and more contribution from the vertical component, the 2D data may be less sensitive to seismic anisotropy. However, the bin size perpendicular to the 2D profile over which amplitudes are summed is 1 km which assumes that lateral variations in structure and rock physical properties are negligible over this distance. This is obviously not true for the Lower Seve Nappe and the lower reflection continuity in the 3D may be more representative of the true structure in the unit. A proper solution for calculating and applying both residual statics and DMO corrections on the 3D data set may improve the coherency of reflections within the Lower Seve Nappe.

4.3. Interpretation

The combination of the 3D seismic data and the borehole geophysical logging allows for an interpretation of the structure of a lower section of the Middle Allochthon in the Swedish Caledonides. Fig. 11 shows inline 1052 and crossline 1104 from the migrated and depth-converted seismic volume with some of the major horizons delineated. The seismic section has been divided into three parts and these are discussed in detail below; 1) The Lower Seve Nappe above the high strain zone (above S.Z. in Figs. 9A, 10 and 11), 2) the high strain zone, interpreted as the basal thrust zone (S.Z.), and 3) deeper structures (below U1).

4.3.1. The Lower Seve Nappe

The Lower Seve Nappe is highly reflective throughout but suffers from low lateral continuity of reflections and unsampled regions owing to the complex geology and limited acquisition. Some of the stronger reflective zones may be due to mafic boudins (e.g. Fig. 3A) that, depending on their geometrical shape, may not produce single continuous reflections for the measured signal frequencies. The lithological and geophysical variations observed on the core and in the borehole can nevertheless be correlated with some of the more prominent reflections by inspection of the entire 3D volume (Fig. 11). For the purpose of visualization, however, the discussion of reflections within the Lower Seve Nappe is referenced to inline 1045 in Fig. 9A.

The shallowest reflection, cutting the COSC-1 borehole subhorizontally around 200 m (S1 in Fig. 9A), can be correlated with a sharp negative spike in both v_p and density, followed by a strong increase in v_p. Just above 200 m depth there is a transition from weathered calc-silicate gneiss, containing (possibly water-bearing) fractures and micro-karst with associated high porosity, into more unaltered gneiss with mylonitic bands and the occurrence of an about 4 m thick unit of amphibolite and amphibole gneiss (Fig. 9B). A second, shallowly SW dipping, reflective package (S2 in Fig. 9A) intersects the borehole at around 300 m depth where banded gneisses and migmatites have been mapped.

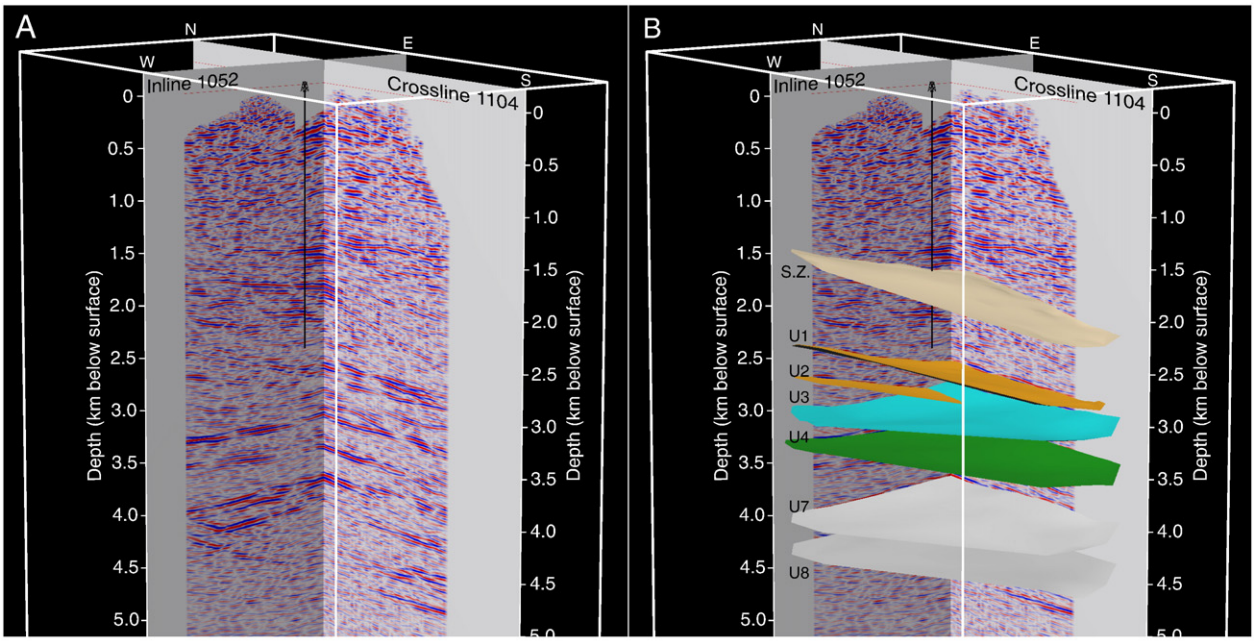

Fig. 11. Inline 1052 and crossline 1104 are shown in A) and again with interpreted horizons in B). The top of the shear zone (S.Z.) was picked along reflections intersecting the borehole at about 1700 m in accordance with the present interpretation of the core although reflections within 200 m directly above have similar apparent geometry. Whereas the reflections within the interpreted basal shear zone dip towards the southeast, reflection U1 and U2 only dip towards east and underlying interfaces (U3 and below) are subhorizontal to slightly west dipping. Depth is referenced to the surface elevation at COSC-1 (523 m above sea level).

Between reflections S3 and S5 is a complex pattern of strong reflections which are apparently dipping at about 10–15° towards the west (Fig 9A). At corresponding depths in the core (Fig. 9B), high-density mafic lenses occur intermittently within the felsic gneisses and calc-silicates, increasing in both frequency and thickness down to reflection S4 at a depth of about 750 m. Below this the mafic units become less abundant down to about 1.2 km depth. Reflection S6 may be related to the negative spike in v_p at about 1.2 km which is, once more, likely associated with micro-karst and possible fluid flow.

At about 1.45 km depth, where north-west dipping S7 is truncated by a south-east dipping reflective package S8, the core reveals a complicated succession of amphibolite, mylonite, gneiss, marble and mica-schist (Fig. 9B). S8 appears to follow parallel to the interpreted basal shear zone and merge with it at the southeastern edge of the cube where they (as seen in the 2D data in Fig. 10) turn into a thinner north-west dipping reflective package that reaches the surface in the vicinity of the boundary between the Lower Seve Nappe and underlying units.

The contrast in deformation observed between the gneiss/calc-silicate rocks to that of amphibolite likely represents a rheological difference in these two units. Ductile deformation characteristics are apparent, in the form of strong crystallographic preferred orientation (CPO) of quartz, feldspar and mica in the gneisses and hornblende in amphibolite (Czaplinska et al., 2015). However, the boudinage of amphibolite indicates that this lithology is competent and strong in comparison to the weaker more ductile gneiss/calc-silicate rocks. This may reflect the deformation conditions during the late stages of the Lower Seve emplacement as the complex gradually cooled. The generally strong CPO of anisotropic crystals, such as hornblende and mica, indicates that seismic wave velocities should also be highly anisotropic. Modeling and laboratory measurements of seismic properties indicate that P wave velocity anisotropy ranges from ~5% in the felsic gneisses/calc-silicates up to ~12% in the amphibolites (Czaplinska et al., 2015; Wenning et al., 2015).

4.3.2. The SNC basal shear zone

The shear zone is interpreted to begin at 1710 m depth in the COSC-1 borehole where mylonite bands are observed in the core with increasing frequency and thickness, implying increasing strain (S.Z. in Figs. 9A, 10 and 11). In contrast to the reflectivity in the Lower Seve Nappe, with frequent impedance contrasts and limited lateral extent, reflections associated with the interpreted zone at the base of the SNC are in general well defined and continuous over longer distances. The zone appears to dip uniformly towards the southeast at about 12°. The borehole did not penetrate the base of the zone and therefore its thickness is unknown. Recrystallized metasandstones appear occasionally in the lowermost 200 m in the borehole and may suggest a transition into lithologies of underlying tectonic units. The c. 400 m thick zone of weaker reflectivity (from c. 2300 m to 2700 m in Fig. 9A), possibly linked with a composition of mylonites, felsic rocks and metasandstones, suggests that the shear zone extends another 200 m below the COSC-1 borehole. It is underlain by the strong reflective package U1 found at 2.7 km depth (Figs. 9A, 10 and 11) which dips mainly eastwards at about 11 degrees (Fig. 11). This package is therefore interpreted to be related to underlying tectonic units, implying that the shear zone has a thickness of c. 1 km.

Several differences between the basal shear zone and the overlying Lower Seve Nappe are apparent, especially in terms of the physical properties and chemical composition (Lorenz et al., 2015b). The large thickness of the basal shear zone implies that its deformation is broadly distributed. However, localization of strain and grain-size reduction in highly strained zones, separated by lenses of less deformed rocks, indicates that deformation is not uniformly distributed throughout this more than 800 m thick shear zone. Note that outcrops of phyllonite and meta-arkose have been identified west of the Åreskutan mountain (e.g. Arnbom, 1980; Helfrich, 1967). In a modified sketch drawing based on a cross-section of Helfrich (1967); Arnbom (1980) indicated that the phyllonite – meta-arkose unit dips gently towards the east at the western edge of Åreskutan mountain, continuing underneath and leveling off to become subhorizontal in the location that roughly corresponds to the drill site of COSC-1. Qualitatively, the description of this phyllonite – meta-arkose unit (Arnbom, 1980) fits well with the lithologies encountered in the lower 200 m of the COSC-1 drill core, where both metasandstones and phyllosilicate-rich mylonites are encountered. The lithologies of this unit were tentatively assigned to the Särv

Nappe by Arnbom (1980), or as a strongly sheared layer that represents the boundary between the Lower Seve Nappe and the Särv Nappe.

4.3.3. Deeper structures

No information is available below the shear zone at the base of the COSC-1 borehole that can provide constraints on the structures or lithologies present there and that cause the observed reflectivity. Reflections are, however, strong and continuous, even in low fold areas, and observed down to nearly 9 km. As seen in Fig. 11, the reflections below the interpreted basal shear zone of the SNC dip mainly towards east or west, whereas little or no dip component is observed in the north–south direction.

Below the interpreted shear zone is another system of strong reflections bounded at the top by reflection U1 that has a dip more restricted to the east–west direction (Figs. 10 and 11). Both U1 and the underlying sub-parallel reflection U2 are terminated by synformal reflection U3 which is subhorizontal in the west and westwards dipping in the east. Bounded by U1 and U3, a western lithological complex, containing two main units separated by U2, appears to pinch out. U3 appears to be the top of a several hundred meters thick reflective zone of nearly uniform thickness, bounded at its base by the very prominent reflection U4.

Beneath 3.5 km, nearly all reflections appear to be continuous (although disturbed by imperfect merging of the data subsets) across the cube, such as the strong reflections U7 and U8 located at around 3.8–4.4 km depth. A complex system of cross-cutting reflections are observed below about 6 km with an east–west dip component ranging from about 18°E to 12°W (Fig. 10).

In the previous interpretation by Hedin et al. (2012), the zone of weaker reflectivity directly above U1, at the base of the interpreted basal shear zone, was attributed to tightly folded Ordovician turbidites in the uppermost Lower Allochthon which are apparently seismically transparent to the east of the SNC. The prominent reflections U1 to U4 were attributed to repetitions of Cambrian shales and Cambrian to Neoproterozoic sedimentary successions derived from the Baltica platform. Underlying structures related to reflections U5 to U7 were interpreted as allochthonous basement-derived units of acid volcanic rocks (Hedin et al., 2012), also included in the Lower Allochthon. This interpretation was based on geological mapping in windows along the Mullfjället and Olden-Oviksfjäll Antiforms to the west and east of the Åre Synform, respectively, where this succession is observed (Fig. 2). The prominent west-dipping reflection U8 was interpreted as the main décollement with an associated layer of alum shales separating the Caledonian allochthons from the Precambrian autochthonous basement. Reflectivity in the basement could be related to either orogenic deformation during the Caledonian or older Sweconorwegian orogenies or to mafic dyke intrusions similar to those found to the east of the orogenic front (1.2 Ga, Söderlund et al., 2006) or in drill holes to the south (1.0 Ga, Juhlin, 1990).

However, an alternative interpretation is possible. The Särv and Offerdal Nappes are found on the surface along the western margin of the SNC (Fig. 2; Arnbom, 1980), varying in thickness from hundreds of meters to a few kilometers, and overlie the Ordovician turbidites. On the eastern side of the SNC, only traces are found suggesting that they are cut out underneath the SNC. They are thus candidates for the possible lithological units between U1 and U3 (Figs. 9A, 10 and 11). One possibility involves normal faulting along the narrow northwest dipping contact between the SNC and Lower Allochthon in the eastern limb of the Åre Synform, similar to what is observed on the western limbs of the Skardöra and Mullfjället Antiforms further west (Gee, 1988). In this case, the narrow northwest dipping contact may not be a continuation of the thick southeast dipping shear zone, S.Z., encountered in the COSC-1 borehole (as in Fig. 10), but rather truncate it and continue with a northwestwards dip into the deeper reflections.

Furthermore, extensions of the COSC 2D reflection seismic profile (Juhlin et al., 2015) and a magnetotelluric (MT) survey along the entire COSC 2D profile (Yan et al., 2016) were recently acquired. The latter show a very strong signature attributed to the highly conductive alum shales that can be correlated with continuous subhorizontal reflections at about 1 km depth throughout the entire 2D seismic profile to the east of the SNC. The strong conductor in the MT data cannot be followed below the SNC, but the associated reflections dip in underneath it and enter the eastern edge of the 3D seismic cube around reflection U4 (Fig. 10). All along the orogenic front, and in basement windows, Cambrian alum shales are found to rest unconformably on top of the Precambrian basement and may have acted as a lubricant to help facilitate the shallow angle thrusting along the basal detachment.

Anomalies in aeromagnetic data (acquired by the Geological Survey of Sweden in 2011), can be interpreted along the seismic profile using Peter's Half-Slope method (e.g. Reynolds, 2011). This constrains the depth to an assumed highly magnetic Precambrian rock in the basement to depths of around 1 to 1.3 km to the east of the SNC (Juhlin et al., 2016), also approximately coinciding with the extension of reflection U4. Thus, based on these additional geophysical constraints, reflection U4 in the seismic 3D volume is interpreted as the main detachment in which case all underlying reflectivity would be related to deformation and/or structures in the basement. The geophysical data do not, however, rule out the presence of additional major detachments at deeper levels, as in the interpretation of Hedin et al. (2012).

5. Conclusion

The new 3D data provide previously unavailable information on the 3D geometry of the structures both within the SNC as well as on deeper reflectors down to 9 km. The SNC is a geometrically and lithologically complex unit with large variations in rock physical properties and significant seismic anisotropy. Interfaces capable of producing reflections occur with separation much less than the reflection seismic resolution and with conflicting dips, which puts high demands on the processing. Although it is possible to follow the general geometry of reflective packages through the seismically imaged 3D volume, it is presently difficult to follow single reflections over more than a couple of hundred meters. This could be due to either the complex geology or the processing. The technique for calculating and applying both static and moveout corrections is still not optimized and a proper solution may give a better image, especially within the Lower Seve Nappe. Nevertheless, correlation with a simplified geological section, sonic and density logs as well as independently acquired and processed 2D reflection seismic data show good agreement.

The abundance of interfaces with significant impedance contrasts and conflicting dips in the uppermost parts of the Lower Seve Nappe is in marked contrast to the more continuous and well defined reflections within the interpreted basal shear zone. This zone, found to be more than 800 m thick in the COSC-1 core has a nearly uniform thickness throughout the seismic volume and a c. 12° dip towards the southeast. The COSC-1 borehole did not penetrate the base of the shear zone and its true thickness is not known. Metasediments become more frequent in the lowermost 200 m of the COSC-1 core and the seismic section appears much less reflective at this depth. Underlying reflections, at a depth of 2.7 km beneath the COSC-1 drill site, have a different character and could be related to an underlying allochthonous unit, giving the shear zone a thickness of c. 1 km. The basal shear zone can be followed into the COSC 2D reflection seismic profile where it turns upwards and projects towards the boundary between the SNC and Lower Allochthon at the surface. Alternatively, the northwestwards dipping contact between the SNC and Lower Allochthon found at the surface may represent an extensional fault that truncates the southeast dipping basal shear zone of the Lower Seve Nappe.

Presently, the interpretation of the lithologies and structures underneath the SNC and the bottom of the COSC-1 borehole is non-unique. Possibly, the lowermost units of the Middle Allochthon, Särv and Offerdal, underlie the SNC in the west and pinch out at 3 km depth

between the interpreted SNC basal shear zone and units of the Lower Allochthon. The latter is in turn separated from the Precambrian basement by a main décollement and associated alum shales that may be attributed to either the prominent west dipping reflection U8 at a depth of about 4.3 km (following Hedin et al., 2012) or the strong and continuous subhorizontal reflection U4 at a depth about 3.4 km (considering new geophysical constraints).

Acknowledgements

The COSC project is a part of the Swedish Deep Drilling Program (SDDP) which operates within the framework of the International Continental Scientific Drilling Program (ICDP) and the 3D seismic reflection component of the project was partly funded by the Swedish Research Council (VR, grant 2013–5780). The VSP component was led by the Institute of Geophysics and Geoinformatics at TU Bergakademie Freiberg, Germany and the Scientific Drilling group at GFZ Potsdam, Germany with research grants from the German Research Foundation (DFG, grants BU1364/10–1 and GI982/2–1). Hans Palm (HasSeis) planned and oversaw the seismic acquisition.

COSC-1 was financed by the International Continental Scientific Drilling Program (ICDP) and the Swedish Research Council (VR, grant 2013-94). Lund University, Sweden and the ICDP Operational Support Group conducted the downhole logging at the COSC-1 drill site and the latter also supported the VSP experiment. The core was scanned onsite by the COSC-1 science team using the standard Geotek Multi Sensor Core Logger (MSCL-S, provided by the ICDP) and post drilling using the Minalyze CS XRF scanner at Minalyze AB in Göteborg, Sweden.

GLOBE Claritas™ under license from the Institute of Geological and Nuclear Sciences Limited, Lower Hutt, New Zealand was used to process the seismic data. Seismic figures were prepared with GMT from P. Wessel and W. H. F. Smith and GOCAD under academic license from the GOCAD Consortium and Paradigm.

H. Lorenz and D. Gee are thanked for valuable feedback. J. Alcalde and one anonymous reviewer are thanked for constructive criticism that helped improve this manuscript.

References

Adam, E., Perron, G., Milkereit, B., Wu, J., Calvert, A.J., Salisbury, M., Verpaelst, P., Dion, D.-J., 2000. A review of high-resolution seismic profiling across the Sudbury, Selbaie, Noranda, and Matagami mining camps. Can. J. Earth Sci. 37, 503–516. http://dx.doi.org/10.1139/e99-064.

Andersen, T.B., 1998. Extensional tectonics in the Caledonides of southern Norway, an overview. Tectonophysics 285, 333–351. http://dx.doi.org/10.1016/S0040-1951(97)00277-1.

Arbaret, L., Burg, J.-P., Zeilinger, G., Chaudhry, N., Hussain, S., Dawood, H., 2000. Pre-Collisional Anastomosing Shear Zones in the Kohistan arc, NW Pakistan. In: Khan, M.A., Treloar, P.J., Searle, M.P., Jan, M.Q. (Eds.), Tectonics of the Nanga Parbat Syntaxis and the Western Himalaya. Geol. Soc. London, Spec. Publ. 170, pp. 295–311. http://dx.doi.org/10.1144/GSL.SP.2000.170.01.16.

Arnbom, J.-O., 1980. Metamorphism of the Seve Nappes at Åreskutan, Swedish Caledonides. GFF 102 (4), 359–371. http://dx.doi.org/10.1080/11035898009454493.

Asklund, B., 1960. The geology of the Caledonian mountain chain and of adjacent areas in Sweden. Sveriges Geologiska Undersökning, Ba 16.

Bergman, S., Sjöström, H., 1997. Accretion and lateral extension in an orogenic wedge: evidence from a segment of the Seve-Köli terrane boundary, central Scandinavian Caledonides. J. Struct. Geol. 19, 1073–1091. http://dx.doi.org/10.1016/S0191-8141(97)00028-X.

Cheraghi, S., Malehmir, A., Bellefleur, G., 2012. 3D imaging challenges in steeply dipping mining structures: new lights on acquisition geometry and processing from the Brunswick no. 6 seismic data, Canada. Geophysics 77, WC109. http://dx.doi.org/10.1190/geo2011-0475.1.

Corfu, F., Gasser, D., Chew, D.M., (Eds.) 2014. New Perspectives on the Caledonides of Scandinavia and Related Areas, Geol. Soc. London, Spec. Publ. 390. ISBN: 978–1-86239-377-6.

Cosma, C., Enescu, N., 2001. Characterization of fractured rock in the vicinity of tunnels by the swept impact seismic technique. Int. J. Rock Mech. Min. Sci. 38, 815–821. http://dx.doi.org/10.1016/S1365-1609(01)00046-6.

Czaplinska, D., Piazolo, S., Almqvist, B., 2015. Seismic anisotropy in the lower crust: the link between rock composition, microstructure, texture and seismic properties. Geophys. Res. Abstr. 17 (EGU2015-1666).

Dyrelius, D., 1980. Aeromagnetic interpretation in a geotraverse area across the central Scandinavian Caledonides. GFF 102 (4), 421–438. http://dx.doi.org/10.1080/11035898009454498.

Dyrelius, D., 1986. Gravity and magnetics in the central Scandes. GFF 108 (3), 278–280. http://dx.doi.org/10.1080/11035898609454705.

Dyrelius, D., Gee, D., Gorbatschev, R., Ramberg, H., Zachrisson, E., 1980. A profile through the central Scandinavian Caledonides. Tectonophysics 69, 247–284. http://dx.doi.org/10.1016/0040-1951(80)90213-9.

Ebbing, J., England, R.W., Korja, T., Lauritsen, T., Olesen, O., Stratford, W., Weidle, C., 2012. Structure of the Scandes lithosphere from surface to depth. Tectonophysics 536-537, 1–24. http://dx.doi.org/10.1016/j.tecto.2012.02.016.

Elming, S.-Å., 1988. Geological modelling based on gravity data from the central part of the Swedish Caledonides. GFF 110 (4), 317–327. http://dx.doi.org/10.1080/11035898809452666.

England, R.W., Ebbing, J., 2012. Crustal structure of central Norway and Sweden from integrated modelling of teleseismic receiver functions and the gravity anomaly. Geophys. J. Int. 191, 1–11. http://dx.doi.org/10.1111/j.1365-246X.2012.05607.x.

Fossen, H., 2000. Extensional tectonics in the Caledonides: synorogenic or postorogenic? Tectonics 19, 213–224. http://dx.doi.org/10.1029/1999TC900066.

Gee, D.G., 1975. A tectonic model for the central part of the Scandinavian Caledonides. Am. J. Sci. A275, 468–515.

Gee, D.G., 1978. Nappe displacement in the Scandinavian Caledonides. Tectonophysics 47, 393–419. http://dx.doi.org/10.1016/0040-1951(78)90040-9.

Gee, D.G., 1988. Thrust tectonics in the Scandes – upper crustal extension during Scandian compression. GFF 110 (4), 390–392. http://dx.doi.org/10.1080/11035898809452682.

Gee, D.G., 2015. Caledonides of Scandinavia, Greenland, and Svalbard☆. Reference Module in Earth Systems and Environmental Sciences. Elsevier Inc. http://dx.doi.org/10.1016/B978-0-12-409548-9.09133-8 (15 pp.).

Gee, D.G., Sturt, B.A., (Eds.) 1985. The Caledonide Orogen - Scandinavia and Related Areas. John Wiley & Sons Ltd., Chichester, Great Britain. ISBN: 0–471-10504-X

Gee, D.G., Kumpulainen, R., Roberts, D., Stephens, M.B., Zachrisson, E., Thon, A., 1985. Scandinavian Caledonides - Tectonostratigraphic Map, Scale 1:2 000 000, Sveriges Geologiska Undersökning, Ba 35

Gee, D.G., Fossen, H., Henriksen, N., Higgins, A.K., 2008. From the early Paleozoic platforms of Baltica and Laurentia to the Caledonide Orogen of Scandinavia and Greenland. Episodes 31, 44–51.

Gee, D.G., Juhlin, C., Pascal, C., Robinson, P., 2010. Collisional Orogeny in the Scandinavian Caledonides (COSC). GFF 132 (1), 29–44. http://dx.doi.org/10.1080/11035891003759188.

Gee, D.G., Janák, M., Majka, J., Robinson, P., van Roermund, H., 2013. Subduction along and within the Baltoscandian margin during closing of the Iapetus Ocean and Baltica-Laurentia collision. Lithosphere 5 (2), 169–178. http://dx.doi.org/10.1130/L220.1.

Gee, D.G., Ladenberger, A., Dahlqvist, P., Majka, J., Be'eri-Shlevin, Y., Frei, D., Thomsen, T., 2014. The Baltoscandian Margin Detrital Zircon Signatures of the Central Scandes. In: Corfu, F., Gasser, D., Chew, D.M. (Eds.), New Perspectives on the Caledonides and Related Areas. Geol. Soc. London, Spec. Publ. 390, pp. 131–155. http://dx.doi.org/10.1144/SP390.20.

Gilotti, J.A., Kumpulainen, R., 1986. Strain softening induced ductile flow in the Särv thrust sheet, Scandinavian Caledonides. J. Struct. Geol. 8, 441–455. http://dx.doi.org/10.1016/0191-8141(86)90062-3.

Grimmer, J.C., Glodny, J., Druppel, K., Greiling, R.O., Kontny, A., 2015. Early- to mid-Silurian extrusion wedge tectonics in the central Scandinavian Caledonides. Geology 43, 347–350. http://dx.doi.org/10.1130/G36433.1.

Gromet, L.P., Sjöström, H., Bergman, S., Claesson, S., Essex, R.M., Andréasson, P.G., Albrecht, L., 1996. Contrasting ages of metamorphism in the Seve nappes: U-Pb results from the central and northern Swedish Caledonides. GFF 118, 36–37. http://dx.doi.org/10.1080/11035899609546308.

Hedin, P., 2015. Geophysical Studies of the Upper Crust of the Central Swedish Caledonides in Relation to the COSC Scientific Drilling Project. *Digital Comprehensive Summaries of Uppsala Dissertations from the Faculty of Science and Technology*, *Acta Universitatis Upsaliensis* 1281, (87 pp.), ISBN: 978–91-554-9320-2.

Hedin, P., Juhlin, C., Gee, D.G., 2012. Seismic imaging of the Scandinavian Caledonides to define ICDP drilling sites. Tectonophysics 554-557, 30–41. http://dx.doi.org/10.1016/j.tecto.2012.05.026.

Hedin, P., Malehmir, A., Gee, D.G., Juhlin, C., Dyrelius, D., 2014. 3D Interpretation by Integrating Seismic and Potential Field Data in the Vicinity of the Proposed COSC-1 Drill Site, Central Swedish Caledonides. In: Corfu, F., Gasser, D., Chew, D.M. (Eds.), New Perspectives on the Caledonides and Related Areas. Geol. Soc. London, Spec. Publ. 390, pp. 301–319. http://dx.doi.org/10.1144/SP390.15.

Helfrich, H.K., 1967. Ein beitrag zur geologie des Åregebietes aus dem zentralen teil der Schwedischen Kaledoniden. Sveriges Geologiska Undersökning, C 612.

Hossack, J.R., Cooper, M.A., 1986. Collision Tectonics in the Scandinavian Caledonides. In: Coward, M.P., Ries, A.C. (Eds.), Collision Tectonics. Geol. Soc. London, Spec. Publ. 19, pp. 285–304. http://dx.doi.org/10.1144/GSL.SP.1986.019.01.16

Hurich, C.A., 1996. Kinematic evolution of the lower plate during intracontinental subduction: an example from the Scandinavian Caledonides. Tectonics 15, 1248–1263. http://dx.doi.org/10.1029/96TC00828.

Hurich, C.A., Palm, H., Dyrelius, D., Kristoffersen, Y., 1989. Deformation of the Baltic continental crust during Caledonide intracontinental subduction: views from seismic reflection data. Geology 17, 423–425. http://dx.doi.org/10.1130/0091-7613(1989)017<0423:DOTBCC>2.3.CO;2.

Juhlin, C., 1990. Interpretation of the reflections in the Siljan Ring area based on results from the Gravberg-1 borehole. Tectonophysics 173, 345–360. http://dx.doi.org/10.1016/0040-1951(90)90229-2.

Juhlin, C., Hedin, P., Gee, D.G., Lorenz, H., Kalscheuer, T., Yan, P., 2016. Seismic imaging in the eastern Scandinavian Caledonides: siting the 2.5 km deep COSC-2 borehole, central Sweden. Solid Earth http://dx.doi.org/10.5194/se-2015-129.

Juhlin, C., Lorenz, H., Almqvist, B., Gee, D., Pascal, C., 2015. ICDP drilling in the Scandinavian Caledonides: plans for COSC-2. Geophys. Res. Abstr. 17, EGU2015–3027.

Juhojuntti, N., Juhlin, C., Dyrelius, D., 2001. Crustal reflectivity underneath the central Scandinavian Caledonides. Tectonophysics 334, 191–210. http://dx.doi.org/10.1016/S0040-1951(00)00292-4.

Klonowska, I., Majka, J., Janak, M., Gee, D.G., Ladenberger, A., 2014. Pressure-Temperature Evolution of a Kyanite-Garnet Pelitic Gneiss from Åreskutan: Evidence of Ultra-High-Pressure Metamorphism of the Seve Nappe Complex, West-Central Jämtland, Swedish Caledonides. In: Corfu, F., Gasser, D., Chew, D.M. (Eds.), New Perspectives on the Caledonides and Related Areas. Geol. Soc. London, Spec. Publ. 390, pp. 321–336. http://dx.doi.org/10.1144/SP390.7.

Klonowska, I., Janák, M., Majka, J., Froitzheim, N., Kośmińska, K., 2015. Eclogite and garnet pyroxenite from Stor Jougdan, Seve Nappe Complex, Sweden: implications for UHP metamorphism of allochthons in the Scandinavian Caledonides. J. Metamorph. Geol. http://dx.doi.org/10.1111/jmg.12173 (accepted article).

Korja, T., Smirnov, M., Pedersen, L.B., Gharibi, M., 2008. Structure of the central Scandinavian Caledonides and the underlying Precambrian basement, new constraints from magnetotellurics. Geophys. J. Int. 175, 55–69. http://dx.doi.org/10.1111/j.1365-246X.2008.03913.x.

Krauß, F., Simon, H., Giese, R., Buske, S., Hedin, P., Juhlin, C., 2015. Zero-offset VSP in the COSC-1 borehole. Geophys. Res. Abstr. 17, EGU2015–3255.

Labrousse, L., Hetényi, G., Raimbourg, H., Jolivet, L., Andersen, T.B., 2010. Initiation of crustal-scale thrusts triggered by metamorphic reactions at depth: insights from a comparison between the Himalayas and Scandinavian Caledonides. Tectonics 29, 1–14. http://dx.doi.org/10.1029/2009TC002602.

Ladenberger, A., Be'eri-Shlevin, Y., Claesson, S., Gee, D.G., Majka, J., Romanova, I.V., 2014. Tectonometamorphic Evolution of the Areskutan Nappe - Caledonian History Revealed by SIMS U-Pb Zircon Geochronology. In: Corfu, F., Gasser, D., Chew, D.M. (Eds.), New Perspectives on the Caledonides and Related Areas. Geol. Soc. London, Spec. Publ. 390, pp. 337–368. http://dx.doi.org/10.1144/SP390.10.

Lorenz, H., Gee, D., Juhlin, C., 2011. The Scandinavian Caledonides – scientific drilling at Mid-crustal level in a Palaeozoic major collisional orogen. Sci. Drill. 11, 60–63. http://dx.doi.org/10.2204/iodp.sd.11.10.2011.

Lorenz, H., Rosberg, J., Juhlin, C., Bjelm, L., Almqvist, B.S.G., Berthet, T., Conze, R., Gee, D.G., Klonowska, I., Pascal, C., Pedersen, K., Roberts, N.M.W., Tsang, C.-F., 2015a. Operational Report About Phase 1 of the Collisional Orogeny in the Scandinavian Caledonides Scientific Drilling Project (COSC-1). ICDP Operational Report. GFZ German Research Centre for Geosciences http://dx.doi.org/10.2312/ICDP.2015.002.

Lorenz, H., Rosberg, J.-E., Juhlin, C., Bjelm, L., Almqvist, B.S.G., Berthet, T., Conze, R., Gee, D.G., Klonowska, I., Pascal, C., Pedersen, K., Roberts, N.M.W., Tsang, C.-F., 2015b. COSC-1 – drilling of a subduction-related allochthon in the Palaeozoic Caledonide orogen of Scandinavia. Sci. Drill. 19, 1–11. http://dx.doi.org/10.5194/sd-19-1-2015.

Majka, J., Be'eri-Shlevin, Y., Gee, D.G., Ladenberger, A., Claesson, S., Konečny, P., Klonowska, I., 2012. Multiple monazite growth in the Åreskutan migmatite: evidence for a polymetamorphic late Ordovician to late Silurian evolution in the Seve Nappe Complex of west-central Jämtland, Sweden. J. Geosci. 57, 3–23. http://dx.doi.org/10.3190/jgeosci.112.

Majka, J., Rosen, Å., Janak, M., Froitzheim, N., Klonowska, I., Manecki, M., Sasinkova, V., Yoshida, K., 2014. Microdiamond discovered in the Seve nappe (Scandinavian Caledonides) and its exhumation by the "vacuum-cleaner" mechanism. Geology 42, 1107–1110. http://dx.doi.org/10.1130/G36108.1.

Milkereit, B., Eaton, D., 1998. Imaging and interpreting the shallow crystalline crust. Tectonophysics 286, 5–18. http://dx.doi.org/10.1016/S0040-1951(97)00251-5.

Okoye, P.N., Uren, N.F., 1992. Spatial resolution in anisotropic media. Explor. Geophys. 23, 255–260. http://dx.doi.org/10.1071/EG992255.

Palm, H., 1984. Time-delay interpretation of seismic refraction data in the Caledonian front, Jämtland, central Scandinavian Caledonides. GFF 106 (1), 1–14. http://dx.doi.org/10.1080/11035898409454597.

Palm, H., Gee, D.G., Dyrelius, D., Björklund, L., 1991. A reflection seismic image of Caledonian structure in central Sweden. Sveriges Geologiska Undersökning, Ca 75.

Park, C.B., 1996. Swept impact seismic technique (SIST). Geophysics 61, 1789–1803. http://dx.doi.org/10.1190/1.1444095.

Pascal, C., Ebbing, J., Skilbrei, J.R., 2007. Interplay between the Scandes and the Trans-Scandinavian Igneous Belt: integrated thermo-rheological and potential field modelling of the central Scandes profile. Nor. Geol. Tidsskr. 87, 3–12.

Rey, P., Burg, J.-P., Casey, M., 1997. The Scandinavian Caledonides and their relationship to the Variscan belt. Geol. Soc. Lond. Spec. Publ. 121, 179–200. http://dx.doi.org/10.1144/GSL.SP.1997.121.01.08.

Reynolds, J. M., 2011. An Introduction to Applied and Environmental Geophysics, 2nd ed., Wiley-Blackwell, Chichester, United Kingdom, ISBN: 978–0-471-48535-3.

Roberts, D., 2003. The Scandinavian Caledonides: Event chronology, palaeogeographic settings and likely modern analogues. Tectonophysics 365, 283–299. http://dx.doi.org/10.1016/S0040-1951(03)00026-X.

Salisbury, M.H., Milkereit, B., Ascough, G., Adair, R., Matthews, L., Schmitt, D.R., Mwenifumbo, J., Eaton, D.W., Wu, J., 2000. Physical properties and seismic imaging of massive sulfides. Geophysics 65, 1882–1889. http://dx.doi.org/10.1190/1.1444872.

Schmidt, J., 2000. Deep Seismic Studies in the Western Part of the Baltic Shield. Acta Univ. Ups., Uppsala Diss. From Fac. Sci. Technol. 24, Uppsala, Sweden (147 pp.).

Simon, H., Krauß, F., Hedin, P., Buske, S., Giese, R., Juhlin, C., 2015a. A combined surface and borehole seismic survey at the COSC-1 borehole. Geophys. Res. Abstr. 17, EGU2015–4554.

Simon, H., Krauß, F., Hedin, P., Buske, S., Giese, R., Juhlin, C., Lay, V., 2015b. The Derivation of an Anisotropic Velocity Model from a Combined Surface and Borehole Seismic Survey at the COSC-1 Borehole, Central Sweden. Abstract H11B-1327 Presented at the 2015 Fall Meeting, AGU, San Fransisco, 14–18 December.

Söderlund, U., Elming, S.-Å., Ernst, R.E., Schissel, D., 2006. The central Scandinavian dolerite group-protracted hotspot activity or back-arc magmatism? Constraints from U-Pb baddeleyite geochronology and Hf isotopic data. Precambrian Res. 150, 136–152. http://dx.doi.org/10.1016/j.precamres.2006.07.004.

Stephens, M.B., Gee, D.G., 1989. Terranes and Polyphase Accretionary History in the Scandinavian Caledonides. In: Dallmeyer, R.D. (Ed.), Terranes in the Circum-Atlantic Paleozoic Orogens. GSA Special Papers 230, pp. 17–30. http://dx.doi.org/10.1130/SPE230-p17.

Strömberg, A., Karis, L., Zachrisson, E., Sjöstrand, T., Skoglund, R., Lundegårdh, P.H., Gorbatschev, R., 1984. Berggrundskarta över Jämtlands län utom förutvarande Fjällsjö kommun, scale 1:200 000. Sveriges Geologiska Undersökning, Ca 53, Uppsala, Sweden.

Törnebohm, A.E., 1888. Om fjällproblemet. GFF 10 (5), 328–336. http://dx.doi.org/10.1080/11035898809444211.

Tsang, C., Rosberg, J., Sharma, P., Niemi, A., Juhlin, C., 2015. Hydrogeologic testing during drilling of COSC-1 borehole : application of FFEC logging method. Geophys. Res. Abstr. 17, EGU2015–4414.

Wenning, Q., Almquist, B., Ask, M., Schmitt, D.R., Zappone, A., 2015. Elastic anisotropy and borehole stress estimation in the Seve Nappe Complex from the COSC-1 well, Åre, Sweden. Geophys. Res. Abstr. 17, EGU2015–6594.

Williams, I.S., Claesson, S., 1987. Isotopic evidence for the Precambrian provenance and Caledonian metamorphism of high grade paragneisses from the Seve nappes, Scandinavian Caledonides - II. Ion microprobe zircon U-Th-Pb. Contrib. Mineral. Petrol. 97, 205–217. http://dx.doi.org/10.1007/BF00371240.

Yan, P., Juanatey, M.A.G., Kalscheuer, T., Juhlin, C., Hedin, P., Savvaidis, A., Lorenz, H., 2016. A magnetotelluric investigation in the Scandinavian Caledonides in western Jämtland, central Sweden, using the COSC-1 borehole log as a priori information. Geophys. J. Int. (in review).

Yilmaz, Ö., 2001. Seismic Data Analysis: Processing, Inversion, and Interpretation of Seismic Data, 2nd ed. Investigations in Geophysics 10, Society of Exploration Geophysicists,. ISBN: 978–1-56080-158-0. (2065 pp.)